scientific reports

Check for updates

OPEN

Network structure-based decorated CPA@CuO hybrid nanocomposite for methyl orange environmental remediation

Dina F. Katowah[1], Sayed M. Saleh[2,3], Sara A. Alqarni[4], Reham Ali[2,5], Gharam I. Mohammed[1] & Mahmoud A. Hussein[6,7]✉

A unique network core–shell hybrid design-based cross-linked polyaniline (CPA), which was coated with CuO nanoparticles (NPs) and decorated with nitrogen-doped SWCNT/GO/cellulose N-SWCNTS-GO-CE, has been fabricated using the oxidative polymerization technique. This hybrid nanocomposite shows excellent photocatalytic degradation and an acceptable adsorption capability for Methyl Orange (MO) dye in aqueous solutions with a very slight effect for the N-SWCNTS-GO-CE CuO component. The prepared nanocomposites were used for the removal of a carcinogenic and noxious dye, Methyl Orange, from aqueous samples under various adsorption conditions. Approximately 100% degradation of 10 mg/L of Methylene orange dye was observed within 100 min at pH 6.0 using 50 mg/L CPA/N-SWCNTS-GO-CE/CuO nanocomposite under UV radiation. Additionally, significant factors were investigated on the degradation process including the contact time, MO initial concentration (C_i), solution pH, and dosage of the CuO nanocomposite. All investigated experiments were performed under UV radiation, which provided significant data for the MO degradation process. Furthermore, the recovery of the nanocomposite was studied based on the photocatalytic process efficiency. The obtained data provide the high opportunity of reusing CPA/N-SWCNTS-GO-CE/CuO nanocomposite for numerous photocatalytic processes. The CPA/N-SWCNTS-GO-CE/CuO nanocomposite was prepared via chemical oxidative copolymerization of polyaniline (PANI) with p-phenylenediamine (PPDA) and triphenylamine (TPA) in the presence of N-SWCNTS-GO-CE and CuO NPs. The morphology, structure and thermal properties of the CPA/N-SWCNTS-GO-CE/CuO nanocomposite were investigated using various techniques, including FTIR, XRD, RAMAN, SEM, MAP, EDX, TEM, TGA and DTG. Therefore, CPA/N-SWCNTS-GO-CE/CuO nanocomposite can be effectively used as a convenient and reusable adsorbent to remove hazardous dye from wastewater.

Harmful and toxic chemicals, pigments, and dyes increase pollution, can cause dangerous effects, and are predicted to increase in quantity in the coming years[1,2]. Most of the dyes are toxic, persistent and non-biodegradable. It causes serious impact on the environment and adversely affects the life of animals and aquatic species. Based on the chemical structure, dyes are classified into three types i.e. anionic (or acid, reactive and direct dye), cationic (basic dyes) and non-ionic dyes (dispersed dyes)[3]. Methyl orange (MO) is one of the azo dyes that are often used as textile dyes and have different structure which depends on the acidity. Non-biodegradable methyl orange can produce several environmental pollution problems by releasing toxic and carcinogenic compounds in the waters even at low concentrations and results in induced lesions and cancers[4]. MO also famous are used in manufacturing and production of printing paper, and act as pH-indicator that convert its colour while protonated is another well-known hydrophobic anion. MO are the one of the compound that categorized in stable compound with

[1]Department of Chemistry, Faculty of Applied Science, Umm Al-Qura University, P.O. Box 16722, Makkah 21955, Saudi Arabia. [2]Department of Chemistry, College of Science, Qassim University, Buraidah 51452, Saudi Arabia. [3]Chemistry Branch, Department of Science and Mathematics, Faculty of Petroleum and Mining Engineering, Suez University, 43721 Suez, Egypt. [4]Department of Chemistry, College of Science, University of Jeddah, Jeddah, Saudi Arabia. [5]Department of Chemistry, Faculty of Science, Suez University, 43518 Suez, Egypt. [6]Department of Chemistry, Faculty of Science, King Abdulaziz University, Jeddah 21589, Saudi Arabia. [7]Polymer Chemistry Lab, Chemistry Department, Faculty of Science, Assiut University, Assiut 71516, Egypt. ✉email: mahussein74@yahoo.com

shows a very low of biodegradability and its dissolved in water contact but have a high percentage of difficulty to eliminate from water bodies by using treatment such as purification process of water within industry or by treatment methods[5]. Studies have been developed for dye elimination from aqueous environments, including diverse methods such as physical, biological, and chemical methods[6]. Adsorption methods are considered the most economical process to eliminate water-soluble toxic and dangerous substances. There are varied adsorbent substances such as clays, biomass, wool fibres, biopolymers, and activated carbon, which have been utilized in water-refining methods. Among conducting polymers, poly(aniline-co-p-phenylenediamine) has attracted a lot of attention due to its simple composition, good electrochemical properties, chemical stability, and hopeful applications in many fields[7]. However, the evolution of CPA properties is challenging. Many researchers have examined the properties of CPA using appropriate materials and different synthetic processes[8]. PANI based nanocomposite materials have been utilized as an efficient sorbent for the photocatalytic degradation of different types of organic pollutants as reported in previously in the literature[9–13]. Cross-linking may be suitable for developing electrical and electrochemical properties of the conductive polymers. Yang et al. prepared cross-linked PANI composites by the in situ chemical oxidative polymerization of aniline in the presence of triphenylamine (TPA) and p-phenylenediamine (PPDA)[14]. Until now, there is no study on the utilization of cross-linked PANI for dye removal. Inorganic nanofiller/polymers are new types of polymeric materials, where inorganic nanofillers are incorporatedinto the polymer matrix[15]. These materials combine the advantages of both components. Among various transition metal oxides, e.g., Fe, Ni, Zn, and Cu, the synthesis of CuO is a significant issue of study. The nanostructure of CuO is especially important because it displays the electron transfer at the lower potential, is non-toxic and is comparatively simple to synthesize with various morphologies and dimensions[16,17]. As a p-type semiconductor, CuO is chemically stable, abundant and inexpensive[18,19]. CuONPs are significant due to their numerous applications in gas sensors[20], biosensors[21], super-capacitor electrodes[8], batteries[18], heterogeneous catalysts[22], photocatalysis[23–25], solar cells[26] and antimicrobial materials[27].Graphene (G) and carbon nanotubes (CNTs) are two of the most fabricated nanomaterials with unique chemical, electronic, optical, electrochemical and mechanical properties. Due to the unusual properties of the two types of carbons, their large surface area, and very effective electrocatalytic behaviour,their combination is the most attractive candidate for environment treatments[28,29]. The use of nanocellulose as reinforcement in nanocomposites has been considered a prevalent study point. In addition to many features of nanocellulose, such as its low density, low cost, low energy consumption, renewability, biodegradability, high appointed features, and comparatively perfect surface reactivity, nanocellulose displays better features as a reinforcing phase in nanocomposites than micro- or macro-cellulose composites. The tailorability, processability, and design flexibility of nanocellulose polymer composites enable comprehensive exploitation in the packaging, automotive, electronics, and biotechnology industries, among others[30].

Water contamination due to chemical compounds from industrial sources is a heavy source of environmental pollution. The main ingredients of these contaminants involve dyes, heavy metals, pesticides, detergents, organic compounds and phenol derivatives[31]. Organic dyes are considerably exhausted in many industrial applications such as coating, photographic, textile dyeing and various types of photo-chemical processes in industry. Most of the dyes used as colouring materials are poisonous to aqueous organisms[32]. Enormous efforts have been spent by many scientists to achieve appropriate treatment protocols to remove contaminants from wastewater that originates from diverse industrial sources[33]. Numerous techniques were utilized for dye removal from wastewater, including adsorption systems[31], membranes[34] and photocatalytic degradation[35]. The degradation of photocatalytic-based metal oxide nanocatalysts is an advanced oxidation process for dye molecules[36]. This technique was used to remove dye molecules from polluted aqueous solution. The photodegradation procedure applies in the presence of UV radiation and significant metal oxide catalyst[37]. Recently, extraordinary developments have been applied in the dye contaminant photodegradation under ultraviolet light[38,39]. Among numerous metal oxides, CuO is one of the appropriate catalysts for this processdue to its photocatalytic activity, reversibility, non-toxicity and physicochemical properties[40–42]. In our previous work, we prepared variable types of polymer nanocomposites with amazing properties: sensors, conductivity, and coating[43–46]. As a continuation of our previous work, the present work aims to fabricate a nanocomposite of cross-linked CPA with N-SWCNTS-GO-CE and CuO NPs by chemical oxidative copolymerization as effective substances for environmental treatment. The CPA/N-SWCNTS-GO-CE/CuO nanocomposite was applied and evaluated as a potential sorbent to remove MO dye from aqueous solutions. The dye concentration, contact time on the adsorption procedure and effect of pH were examined.

Experimental

Materials. p-phenylenediamine (PPDA) was obtained from PDH in UK. Aniline (Ani) was purchased from Shanghai Chemical Reagent Co. Ammonium persulfate (APS) was received from Acros Organics. Triphenylamine (TPA) was obtained from Janssen Chimica (Belgium). Copper oxide (CuO), nitric acid (HNO_3), sulfuric acid (H_2SO_4), urea, ammonia solution, NaOH, ethanol, and cellulose were purchased from Sigma-Andrich (USA). Graphene and SWCNTs were purchased from the XFNANO Advanced Materials Supplier INC. (China). All chemicals and reagents in the investigations were used as obtained. Deionized water was used throughout the examinations.

Instrumentation and techniques. Field emission scanning electron microscopy (SEM Model Quanta 250 FEG, with 30-kV accelerating voltage at 14 × magnification and up to 1,000,000 resolution for Gun.1n) was utilized to examine the morphological features of the produced materials. High-resolution transmission electron microscopy (HR-TEM) (EM-2100, at 25 × magnification and 200 kV) was also utilized to examine the morphological features of these new materials. Fourier transform infrared (FTIR) spectra were displayed by a

JASCO spectrometer over the range of 4000–300 cm^{-1} and used to obtain information on the functional groups of the studied samples. X-ray diffraction (XRD) of the NC crystallinity was examined by using a Bruker model D8 to study the fundamental structures of these nanocomposites. The instrument include reflectometry, high-resolution diffraction, in-plane grazing incidence diffraction (IP-GID), small-angle X-ray scattering (SAXS), and residual stress and texture investigations. Raman spectroscopy measurements were performed by using a Raman spectrometer (Lab. RAM-HR Evolution Horiba Co.) with a single visible spectrometer, which was equipped with an air-cooled open electrode 1024 × 256 pixel CCD detector, a 532 nm He-Cd laser with 1800 grating (450–850 nm), and a 10% ND filter, using an acquisition time of 5 s, 5 accumulations without spike filter and delay time, and a 100 × objective. To detect the absorbance of light wavelengths, the UV–visible recording spectrophotometer Shimadzu-Japan was used. Thermal analyses were detected in the form of TGA and DTG measurements using Shimadzu DTA-50 and TGA-50 systems at a heating rate of 10 °C/min in air. The thermal performance was examined to define the degradation temperature of the NC and their thermal stabilities.

Fabrication process. *Synthesis of GO.* GO was prepared according to a modified Hummers' method[47].

Synthesis of OXSWCNTs. According to the literature, the OXSWCNTs were set up[46]. First, 100 mg of SWCNTs were scattered in a mixture (1:3 v/v) of HNO_3 (70%) and H_2SO_4 (96%).Then, they were ultrasonicated for 4 h. Next, for 2 h at 80 °C, the suspension was refluxed in an oil bath with attractive blending. At that point, deionized water (DIW) was used to dilute the received mixture and dialysed in DIW until the washing arrangement demonstrated pH > 5. Finally, OXSWCNTs were filtered and dried in a stove at 60 °C.

Synthesis of the N-SWCNTs/GO/cellulose hybrid nanofiller. OXSWCNTs/GO 0.3 g was scattered in DIW100 mL and stirred at 90 °C for 2 h. At that point, 25% aqueous ammonia solution and 0.9 g urea were included and consistently stirred for 12 h at 90 °C. First, because of the formation of the OXSWCNTs/GO hybrid, which dissolved when surplus ammonia was added, the above solution became turbid. Then, in vacuum for 12 h at 90 °C, the transparent solution was evaporated. Cellulose was dissolving in 100 mL H_2O and 10 g of NaOH. Next, under continuous stirring for another 12 h, the two mixtures were combined at 90 °C. Finally, using ethanol, the final product was washed and dried at 200 °C for 7 h.

Synthesis of cross-linked PANI (CPA). The required pure cross-linked PANI was synthesized as reported in the literature[48,49].

Synthesis of CPA and CPA/N-SWCNTs-GO-CE/CuO nanocomposites. The chemical copolymerization of cross-linked PANI with N-SWCNTs-GO-CE and CuO was achieved as follows:

In a 250-mL three-neck flask consisting of 120 ml of 0.5 M H_2SO_4, 5% N-SWCNTs-GO-CE was added. Next, for 2 h at room temperature, the mixture was ultrasonicated. Then, 5% CuO, 1.8626 mL of (doubly distilled) ANI, 0.043256 gm of PPDA and 0.049064 gm of TPA were added. The mixture was ultrasonicated for 30 min. Afterwards, the solution was cooled in an ice bath with continuous stirring at 0–4 °C. Then, 5 g of a pre-cooled solution of ammonium persulfate (APS) dissolved in 0.5 M H_2SO_4 40 mL and added dropwise into the previous solution in approximately 30 min with consistent stirring at 0–4 °C under nitrogen N_2 atmosphere for 24 h to maintain the polymerization. Next, using ultracentrifugation, the resulting precipitate was collected. Then, it was washed with DIW numerous times until the filtrate became colourless. Finally, the black fine powder was dried at 60 °C for 24 h. This experiment was repeated for comparison; the pure cross-linked PANI was prepared using an identical method without N-OXSWCNTs-GO-CE and CuO NPs.

Batch method for dye removal. Batch experimentation was afforded to obtain the optimum parameters for the degradation of methyl orange in the presence of the nanocomposite of CPA/N-SWCNTS-GO-CE/CuO as the photocatalyst. The effects of significant variables such as the contact time, pH, nanocomposite dose and initial concentration of methyl orange MO in the medium were exhaustively investigated. To clarify the parameters of the effective reaction, we adjusted one variable at a time. Here, in batch condition, the experiments were conducted with 100 mL 10-mg/mL MO solution in a beaker (250 mL). In the dark, the dye solution with a colloidal suspension of the specified nanocomposite was mixed for 10 min with a magnetic stirrer, and the net solution was centrifuged (4400 rpm/15 min). By using a UV–Vis spectrophotometer, the resulting supernatant was examined. The dye degradation rate was studied using the following equation[50]:

$$R = \frac{C_0 - C_t}{C_0} \times 100$$

where R is the efficiency rate of dye removal, C_0 is the MO dye initial concentration (mg/L), and C_t is the concentration of MO dye after the adsorption process per time t (min).

Results and discussion

In this study, we aimed to fabricate a nanocomposite of cross-linked CPA with N-SWCNTS-GO-CE and CuO NPs. CPA/N-SWCNTS-GO-CE/CuO nanocomposites were prepared using the previous method, which is the chemical oxidative copolymerization of PANI with p-phenylenediamine PPDA and triphenylamine TPA, but in the presence of N-SWCNTS-GO-CE and CuO. Their morphology, structure, and thermal properties of the nanocomposites were examined via several techniques: SEM, TEM, FTIR, XRD, TGA, DTG, RAMAN and dye removal measurements. The result was as follows.

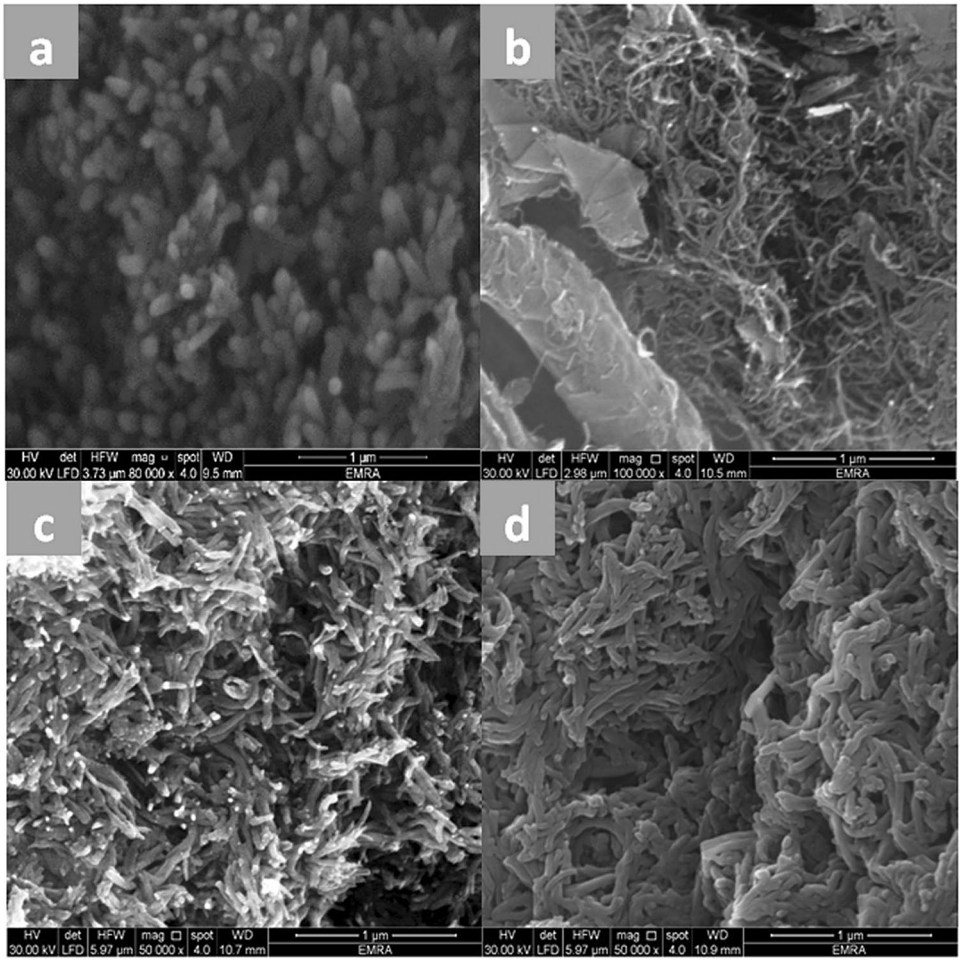

Figure 1. SEM images of CPA (**a**), N-SWCNTs-GO-CE (**b**), CPA/N-SWCNTs-GO-CE (**c**), and CPA/N-SWCNTs-GO-CE/CuO nanocomposites (**d**).

Surface morphology. The surface morphologies of the CPA (a), N-SWCNT-GO-CE (b), CPA/N-SWCNT-GO-CE (c), and CPA/N-SWCNTS-GO-CE/CuO (d) nanocomposites were studied by field emission scanning electron microscopy, as displayed in Fig. 1.The SEM micrographs mainly focus on the morphological modifications,which can be noticed on the surface of the samples[43]. The SEM micrographs further provided evidence of the nanocomposite modification[44]. The morphological parts of the nanocomposites were studied using a Jeol JSM-5400 LV SEM experiment device. The surface of CPA in Fig. 1a displays coral reefs with small holes in the spongy form. N-SWCNT-GO-CE nanofiller SEM images (Fig. 1b) show rod-like particles. These rods are linear (Fig. 1b enlargement X = 100,000). The SEM images of the CPA/N-SWCNT-GO-CE composite displays a surface fabrication upon inundation of N-SWCNTs-GO-CE in its matrix, which is obvious in the enlargement (x = 50,000) in Fig. 1c. The SEM images illustrate the framework with the accumulation of N-SWCNTs-GO-CE on the CPA surface, which prevents many smallhales. In the SEM images of CPA/N-SWCNTS-GO-CE/CuO (Fig. 1d), CPAs coated on CuONPs, which are decorated with N-SWCNTS-GO-CE hybrid composites, form a unique core–shell network.

Figure 2a displays the element mapping of C, N, O, and Cu, which is uniformly distributed in the nanocomposites and proves the presence of N-SWCNTs-GO-CE, CuO and CPA polymers. Figure 2b displays the EDX mapping for the CPA/N-SWCNT-GO-CE/CuO nanocomposites with the peaks of C, N, O, and Cu, which indicate the presence of CuO, N-SWCNTs-GO-CE, and CPA polymer.

Other morphological characteristics for CPA(a), CPA/N-SWCNT-GO-CE(b), CuO(c) and CPA/N-SWCNTS-GO-CE/CuO (d) nanocomposites are specified by TEM as illustrated in Fig. 3. The CPA image shows accumulated layers in Fig. 3a with a scale of 1 µm. TEM images of CPA/N-SWCNT-GO nanocomposites in Fig. 3b show that N-SWCNT-GO-CE nanofillers are instilled in the CPA polymer matrix and almost compose a pulp–shell structure. The black core is the GO nanoparticle, the rods are the SWCNTs; the smooth cortex indicate the polymer matrix. Cellulose nanofibres were decorated on the surface of the mixed NPs and matrix. In Fig. 3c, CuO shows a fibrous form. After N-SWCNTS-GO-CE was mixed with CuO, and CPA, the nanofillers are homogenously distributed and inserted in the CPA polymer, and the mixed N-SWCNTS-GO-CE/CuO are obviously immerged in the CPA polymer matrix (Fig. 3d).

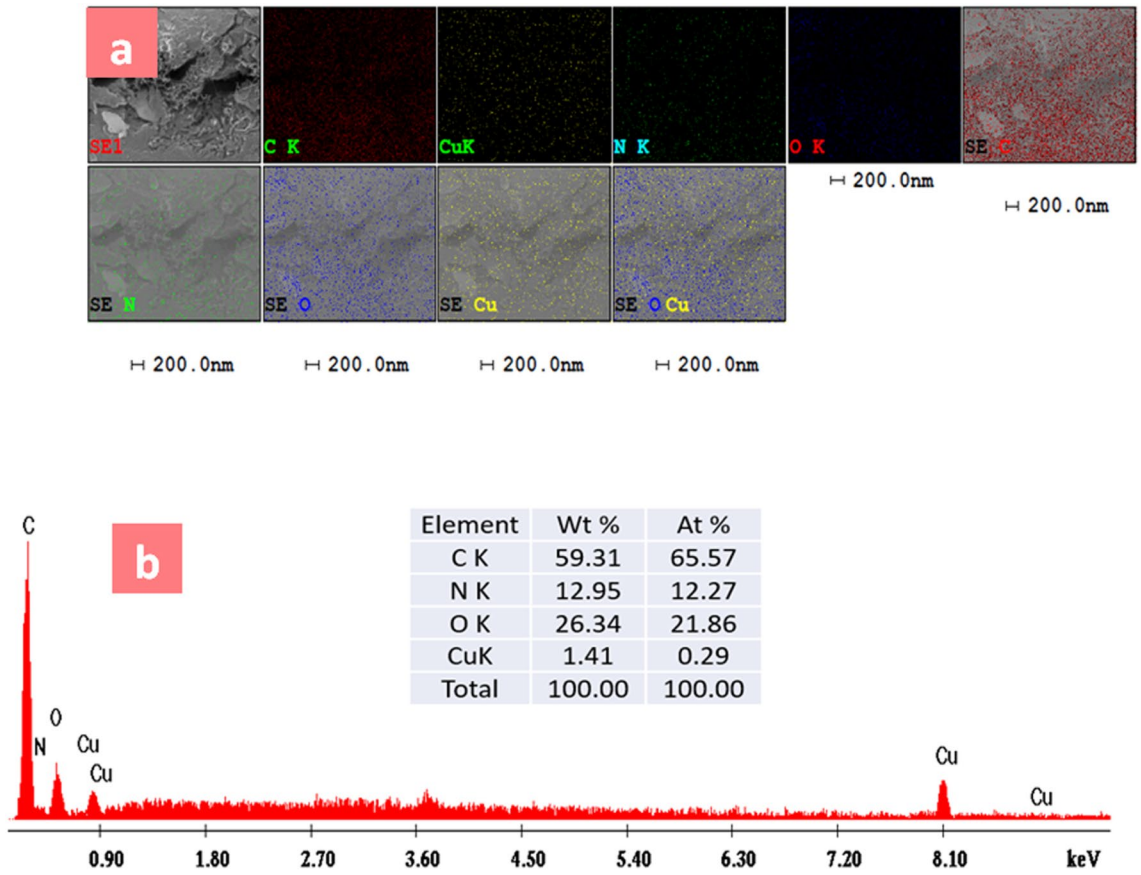

Element	Wt %	At %
C K	59.31	65.57
N K	12.95	12.27
O K	26.34	21.86
CuK	1.41	0.29
Total	100.00	100.00

Figure 2. EDX (**a**) and maps analyzes (**b**) of CPA/N-SWCNTs-GO-CE/CuO nanocomposites.

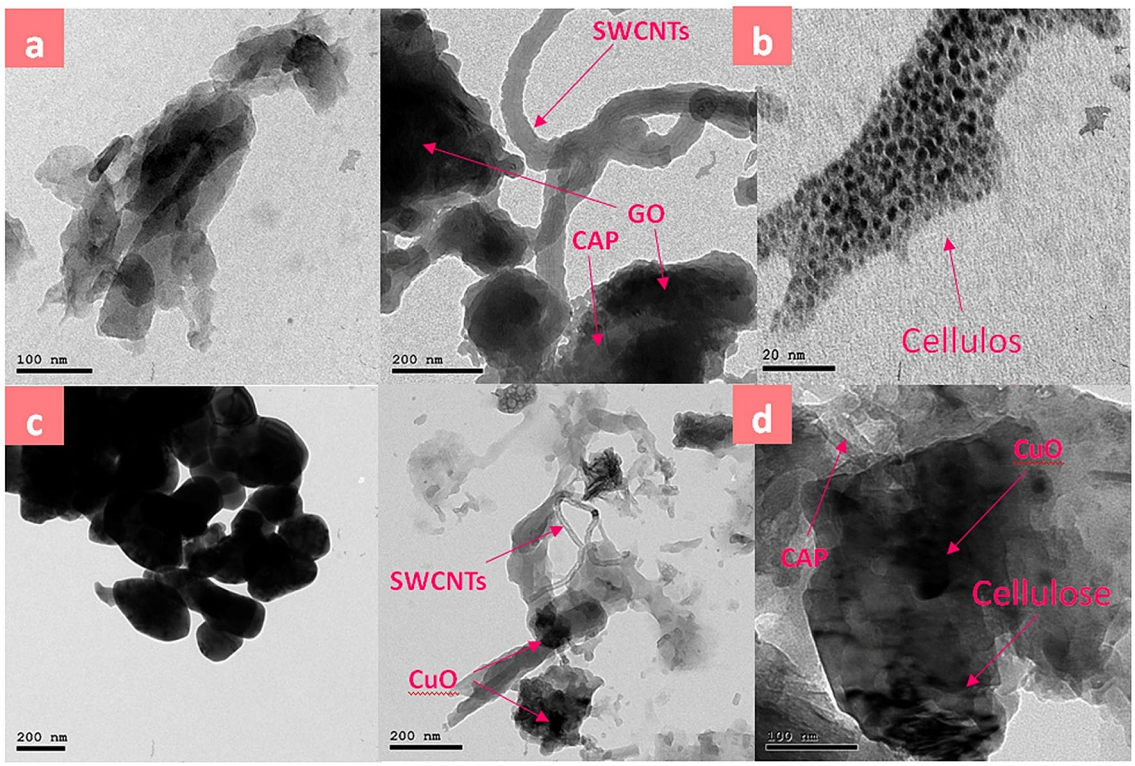

Figure 3. TEM images of CPA (**a**), CPA/N-SWCNTs-GO-CE (**b**), CuO (**c**), and CPA/N-SWCNTs-GO-CE/CuO nanocomposites (**d**).

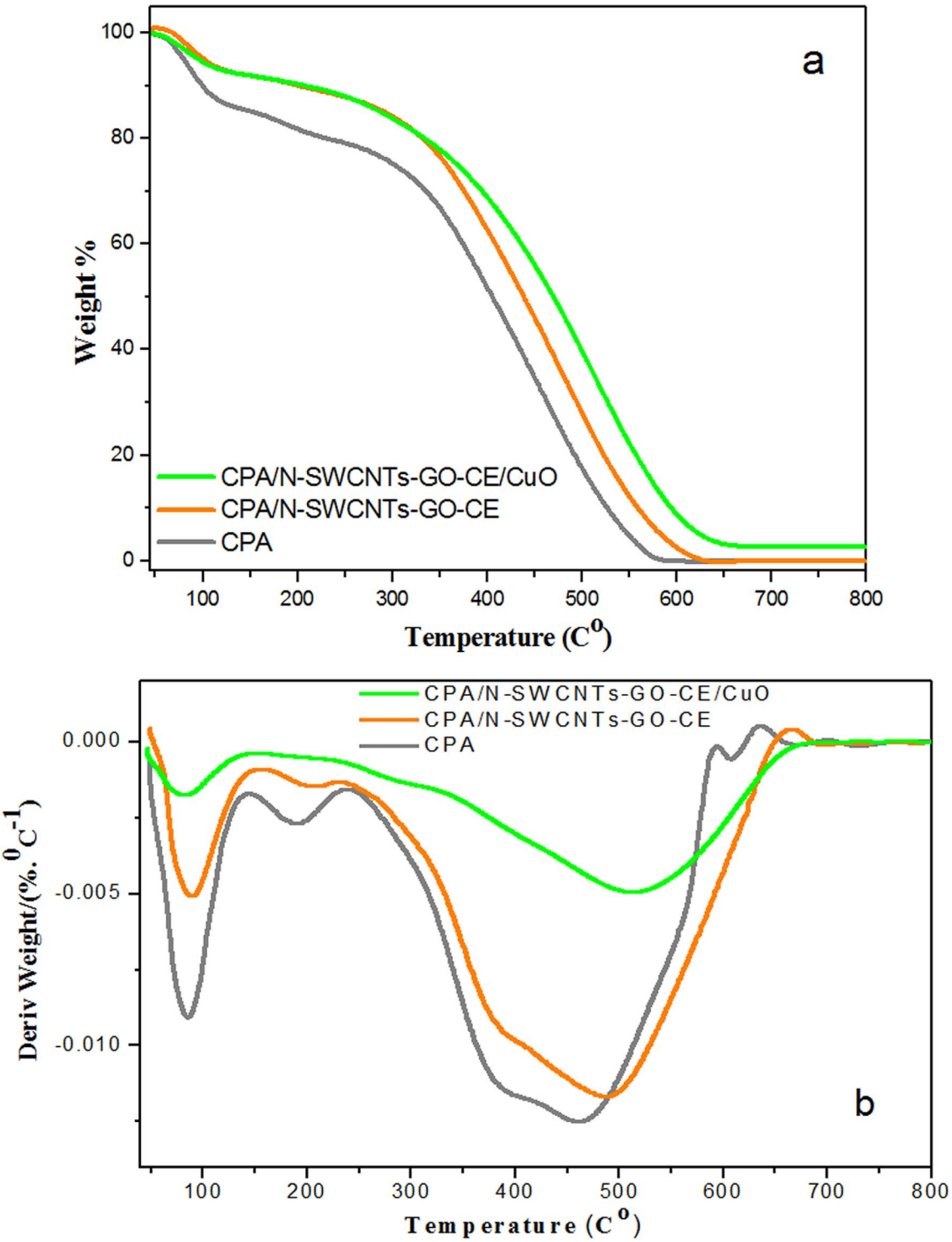

Figure 4. (**a**) TGA curves for pure CPA, CPA/N-SWCNTs-GO-CE and CPA/N-SWCNTs-GO-CE/CuO nanocomposites. (**b**) DTG curves for pure CPA, CPA/N-SWCNTs-GO-CE and CPA/N-SWCNTs-GO-CE/CuO nanocomposites.

Thermal analysis. The thermal attitudes of CPA, fabricated CPA/N-SWCNT-GO-CE, and CPA/N-SWCNTS-GO-CE/CuO nanocomposites were studied by TGA and DTG technique in air at a heating rate of 10 °C min^{-1}, as displayed in Figs. 4a,b. The thermal analysis was performed in a temperature range of 90–800 °C. Table 1 displays the disintegration temperatures for various percentages. The temperatures for10, 25 and 50% weight losses are T_{10}, T_{25} and T_{50}, respectively. The TGA curve display slight weight losses in the range of 95–100 °C, which are more than 5% of the entire weight loss. This weight loss is attributed to the loss of solvents and absorption of moisture and/or water molecules[51,52].

Products	CDT_{max} (°C)	CDT_{final} (°C)	Temperature (°C) for various percentage decompositions		
			T_{10}	T_{25}	T_{50}
CPA	462.44	592.29	541.22	484.08	407.47
CPA/N-SWCNT-GO-CE	492.53	619.38	575.78	514.13	440.48
CPA/N-SWCNTS-GO-CE/CuO	522.35	658.46	614.87	548.69	475.04

Table 1. Thermal behavior of CPA, CPA/N-SWCNT-GO-CE, and CPA/N-SWCNTS-GO-CE/CuO nanocomposites.

Moreover, the TGA analysis of all examined samples shows the role of mixed N-SWCNTS- GO-CE/CuO nanocomposites on the thermal stability of CPA. The TG curves analysis also shows that the studied samples fundamentally decomposed in three decomposition steps. The decomposition begins early in all samples and remain at higher temperatures with decomposition weight loss percentages below 50%. This notice is completely referred to the presence of air atmosphere. The first decomposition step is fundamentally referred to the complete elimination of solvents[14]. The first step was finish at approximately 150 °C and is attributed to the chloride ions linked to the positive positions on the CPA chain, which referred chain degradation. The second decomposition step, which fundamentally occurred at a higher temperature, started at approximately 350 °C and completed at approximately 600 °C and is referred to additional decomposition of CPA chains to smaller chains[52]. Comparable observations are displayed for the CPA/N-SWCNT-GO-CE, and CPA/N-SWCNTS-GO-CE/CuO nanocomposites with small increases in the high temperatures, i.e., increased thermal stability.

Meanwhile, the addition of mixed N-SWCNTS-GO-CE/CuO increases the thermal stability of CPA, which indicates the presence of intermolecular interactions between nanofillers and polymer matrix. T_{10}, T_{25} and T_{50} show important and gradual increases from CPA (the lowest) to CPA/N-SWCNTS-GO-CE/CuO (the highest). From the DTG analysis, the CDT_{max} amount is defined as the maximum temperature at which decomposition occurs[46], i.e., the composite degradation temperature. These amounts are fully identical in all inspected nanocomposites and are approximately 492 °C ± 30.

FT-IR analysis. An FT-IR spectroscopic analysis was investigated from 4000 to 400 cm^{-1}. The acquired spectra for CPA, N-SWCNT-GO-CE, CuO, CPA/N-SWCNT-GO-CE and CPA/N-SWCNT-GO-CE/CuO in FT-IR are displayed in Fig. 5. The FT-IR spectrum of the CPA/N-SWCNT-GO-CE/CuO composite shows the bands associated with pure CPA and N-SWCNT-GO-CE/CuO peaks. In all spectra, broad bands at approximately 3,400 cm^{-1} are attributed to the N–H and C–H stretching modes[53,54]. The two N–H stretching modes are noticed as broad infrared bands with very large intensity (Fig. 5) and attributed to the presence of strong intermolecular H-bonding in molecules[55]. In pure CPA, CPA/N-SWCNT-GO-CE and CPA/N-SWCNT-GO-CE/CuO, a characteristic doublet of bands appears at 1627 and1736 cm^{-1} in the infrared spectrum of aniline and p-PDA[56]. The bands due to the C=O stretch are very prominently observed at 1745 cm^{-1} for the carboxylated SWNT. Other bands are a tiny one at 3452 cm^{-1} and another at 2952 cm^{-1}, which indicate O–H and C–H stretches, respectively. The O–H vibration is related to amorphous carbon because amorphous carbon readily shapes a bond with atmospheric air, and there are C–C vibrations due to the internal disorder. An anti-symmetric stretch C–O is also obvious at 1660 cm^{-1}. The bands at 1236 cm^{-1} and 1405 cm^{-1} indicate C=C[57]. In cellulose, the broad band in the 3602–3110 cm^{-1}region is due to the OH-stretching vibration. The presence of amorphous cellulosic can be ascertained by the shift of the band from 2910 cm^{-1}, which indicates the C–H stretching vibration. Furthermore, the FTIR absorption band at 1420 cm^{-1} is attributed to a symmetric CH_2 bending vibration. The FTIR band at 896 cm^{-1} is attributed to C–O–C stretching[57]. The FT-IR spectra of nanocomposites also display distinguishing bands of GO. Broad bands at1732, 1624, and 3300–3615 cm^{-1} are referred to the C = O stretch of the carboxylic acid group, C=C, and O–H, respectively. The bands at 1226 cm^{-1} refer to the epoxy (C–O) ring stretching, and the bands at 642 cm^{-1}refer to the symmetric ring disfigurement of the epoxy group on the GO nanofillers[15]. In the nanocomposites, there is no remarkable signal for CuO, since the assigned CuO is too small to be detected by FT-IR.

XRD analysis. The expected shape of the prepared nanocomposites has been studied using X-ray diffraction techniques. The XRD characterization styles give a clear evidence for the composite fabrication. XRD diffractograms for CPA, N-SWCNT-GO-CE, CuO, CPA/N-SWCNT-GO-CE and CPA/N-SWCNT-GO-CE/CuO nanocomposites are shown in Fig. 6 over the measuring range of $2\theta = 10–80°$.CPA and N-SWCNT-GO-CE/CuO nanocomposites physically react with each other via the nanocomposite production. The 2θ scan displays the perfect X-ray diffraction patterns for CPA and mixed N-SWCNT-GO-CE/CuO. Figure 6 displays the XRD pattern for mixed N-SWCNT-GO-CE. Three intense peaks at 49°, 33°, and 31°can be ascribed to the crystalline region of N-SWCNTs[58]. Other distinguishing peaks near 30–40° refer to amorphous cellulose[59]. The diffraction peak with a maximum at approximately25° displays the distinguishing composition of GO[60]. For the CuO sample, sharp intense peaks at 2θ of 35.8° and 39.1° conformable to the (111) plane were noticed with other less intense peaks characteristic of CuO.

However, the copolymer CPA displays the XRD patterns with two broad diffraction peaks at $2\theta = 18.4°$ and 26.4°, which are typical of an amorphous substance[58,60] and as illustrated in Fig. 6. These patterns demonstrate a

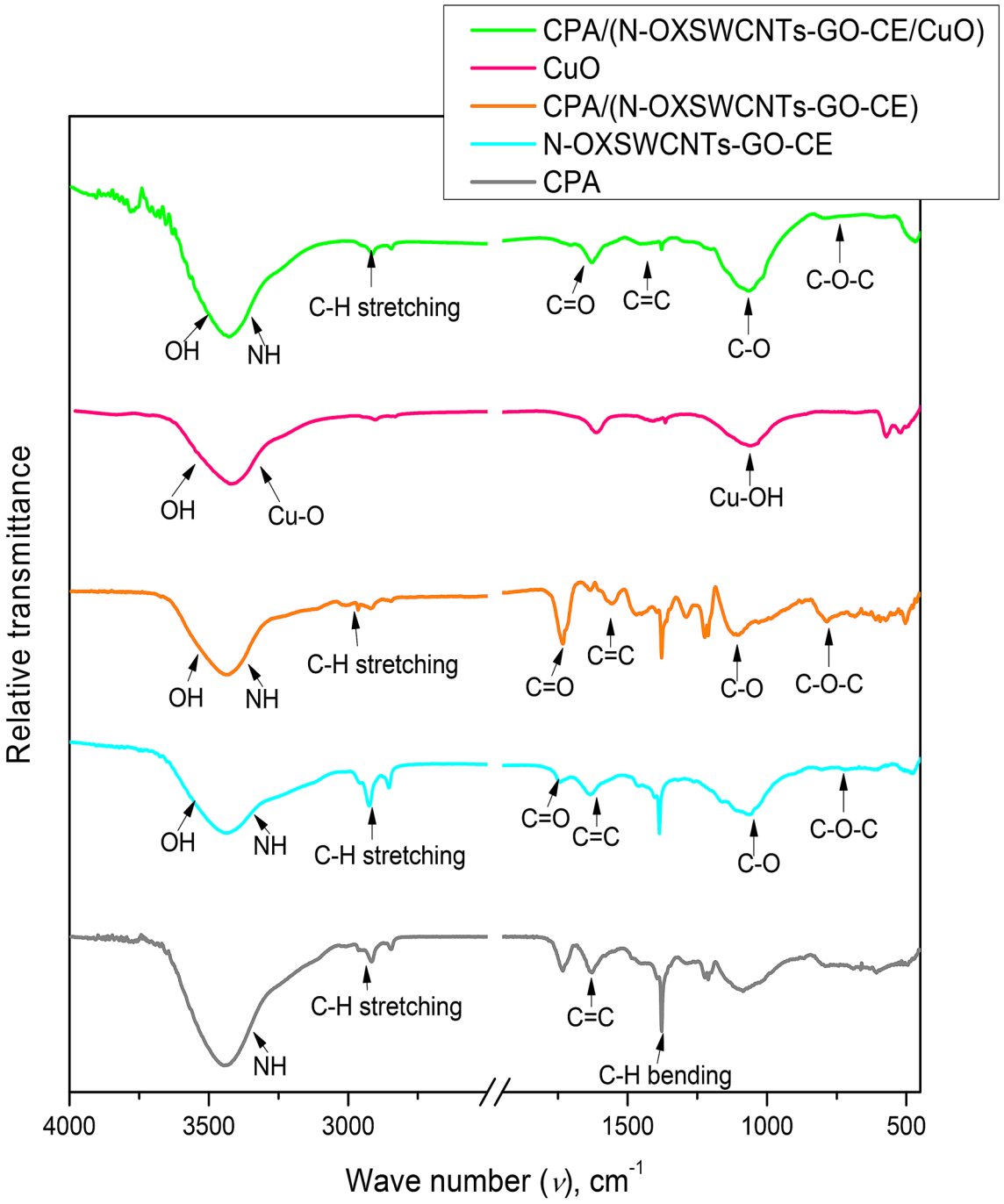

Figure 5. IR spectra for pure CPA, N-SWCNTs-GO-CE, CPA/N-SWCNTs-GO-CE, CuO, and CPA/N-SWCNTs-GO-CE/CuO nanocomposites.

weak degree of crystallinity, since no sharp crystalline beaks are noticed. All of the previous peaks related to the mixed N-SWCNT-GO-CE/CuO and CPA have been mentioned in the XRD pattern for CPA/N-SWCNT-GO-CE/CuO nanocomposites and illustrated in Fig. 6. The XRD diffraction patterns for CPA/N-SWCNT-GO-CE/CuO hybrid nanocomposites are notable with no confusion of the composition of competent nanocomposites. No other crystalline peaks may be specified to another stage or presence of muck in the desirable nanocomposites.

Raman analysis. Raman spectroscopy is applied to prove the presence of N-SWCNTs-GO with CPA in nanocomposites. Figure 7 displays the Raman spectra of N-SWCNTs-GO-CE, CPA/N-SWCNTs-GO-CE, CuO and CPA/N-SWCNTs-GO-CE/CuO nanocomposites. The D band is disorder-induced, e.g., by sp3-hybridized carbon atoms, whereas the G band represents the in-plane stretching E_{2g} mode[61]. The distinctive properties in the Raman spectrum of N-SWCNTs-GO-CE are the so-called D band, which is located at approximately 1340 cm^{-1}, and the G band is located at 1568 cm^{-1}. The G and D peaks of N-SWCNTs-GO-CE appear in the Raman spectra

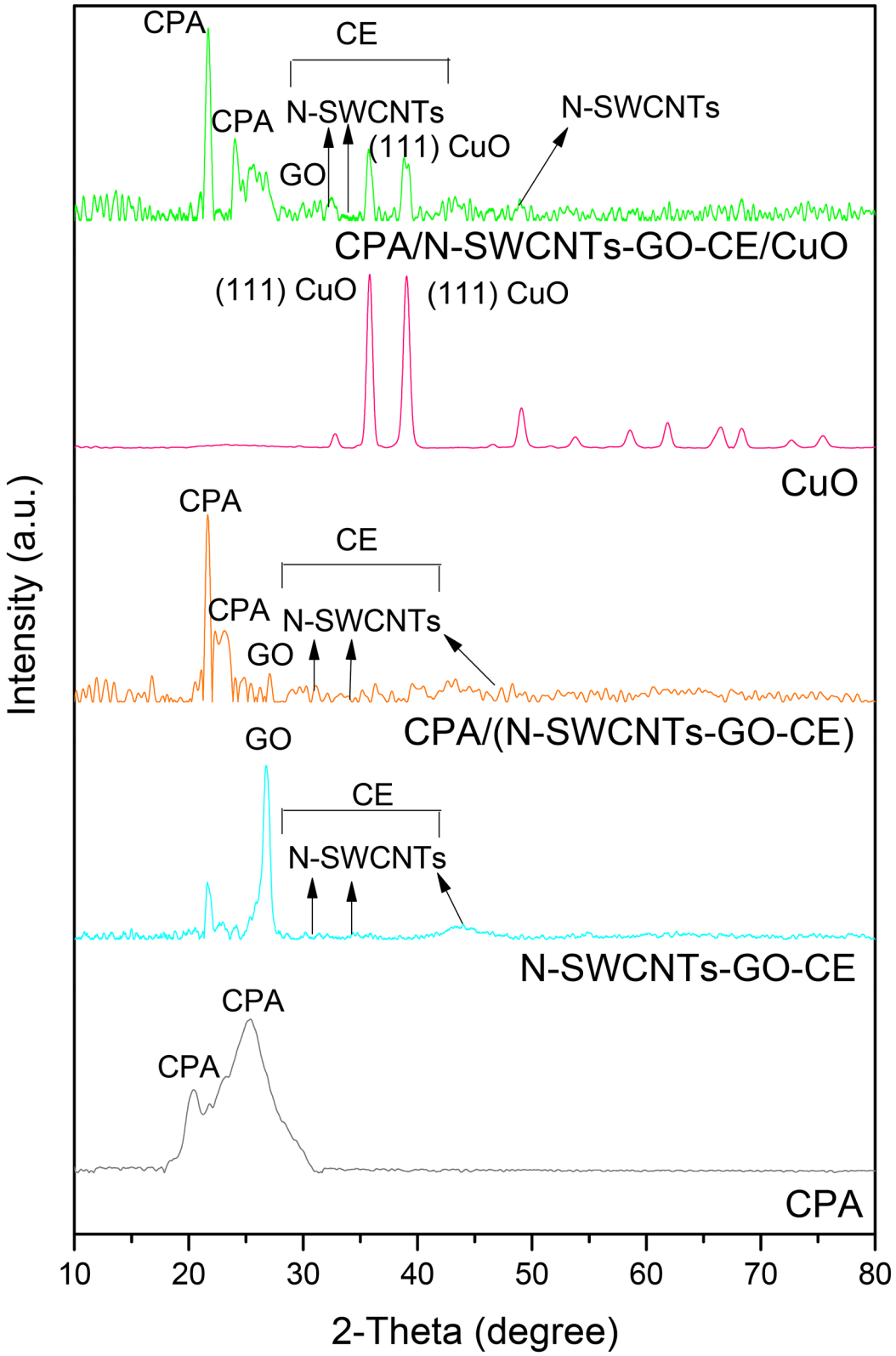

Figure 6. XRD diffraction patterns for pure CPA, N-SWCNTs-GO-CE, CPA/N-SWCNTs-GO-CE, CuO, and CPA/N-SWCNTs-GO-CE/CuO nanocomposites.

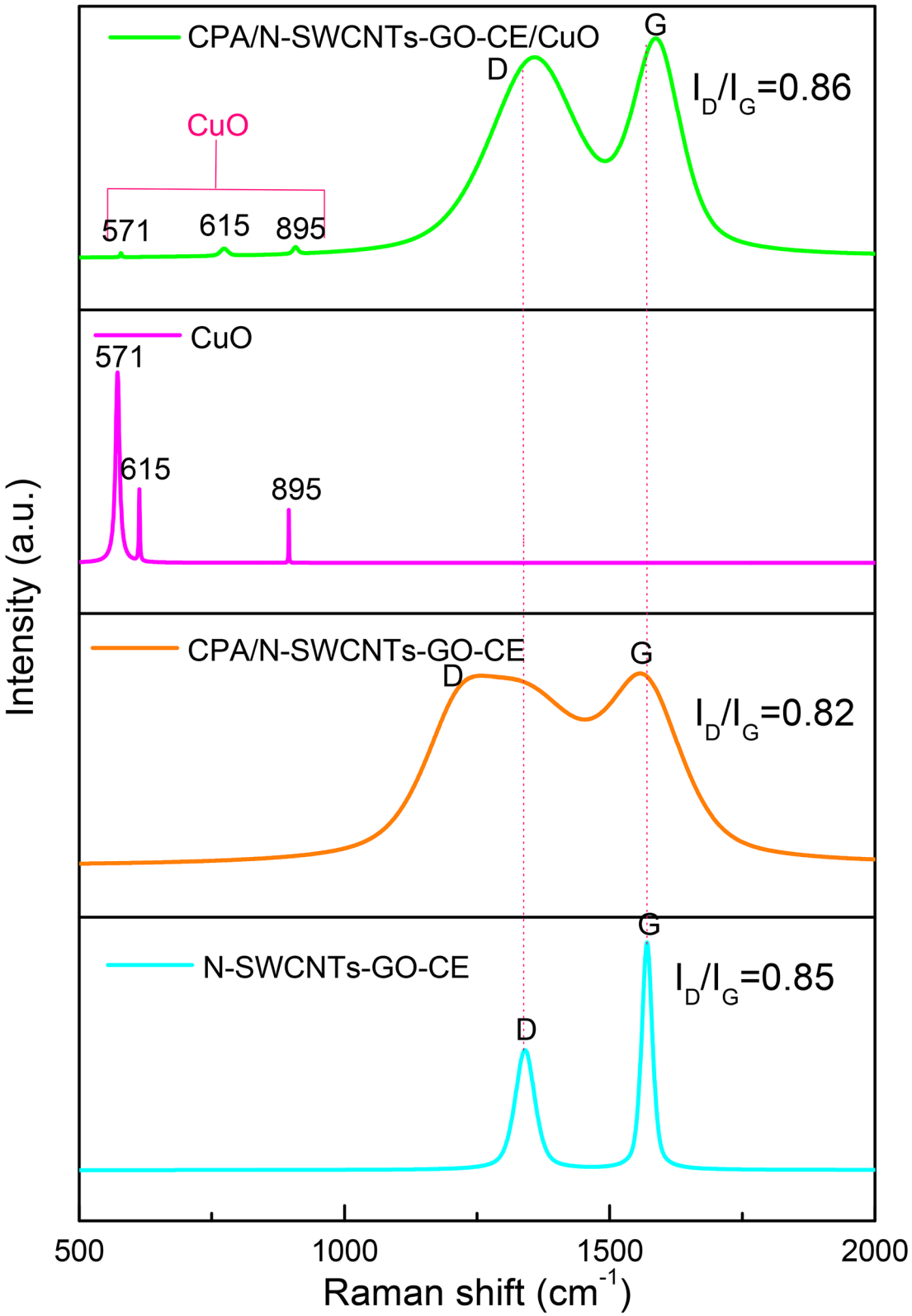

Figure 7. Raman spectrum of N-SWCNTs-GO-CE, CPA/N-SWCNTs-GO-CE, CuO and CPA/N-SWCNTs-GO-CE/CuOnanocomposites.

of CPA/N-SWCNTs-GO-CE nanocomposites. The G and D bands of CPA/N-SWCNTs-GO-CE nanocomposites are slightlydifferent from those of N-SWCNTs-GO-CE and appear at 1571 and 1289 cm^{-1}, respectively. The G and D bands of N-SWCNTs-GO-CE are also present at 1586 cm^{-1} and 1360 cm^{-1} in CPA/N-SWCNTs-GO-CE

nanocomposites and shifted compared with those of N-SWCNTs-GO-CE. The behaviour of all nanocomposites demonstrates that the shift of the G band illustrates a strong interaction between N-SWCNTs-GO-CE and the polymer and possibly a charge transfer between N-SWCNTs-GO-CE and CPA. The expanded G band of nanocomposites mainly refers to the covering effect of amorphous CPA on N-SWCNTs-GO-CE during synthesis[62,63].

The G and D band intensity ratio is a substantial factor to measure the graphitization degree in the required material. The variation in band intensity ratio (I_D/I_G) of the original N-SWCNTs-GO-CE and nanocomposites is a perfect indicator of the proportional grade of defects in N-SWCNTs-GO-CE. If both bands have comparable intensities, there is a high level of structural defects[64]. The I_D/I_G ratios of CPA/N-SWCNTs-GO-CE, and CPA/N-SWCNTs-GO-CE/CuO nanocomposites are 0.85, 0.82 and 0.85. The CPA/N-SWCNTs-GO-CE/CuO nanocomposites has a higher I_D/I_G ratio than N-SWCNTs-GO-CE, which suggests that no defects were created in the N-SWCNTs-GO-CE lattice. Moreover, the peaks at 577–907 cm^{-1} can be ascribed to CuO. These results confirm the presence of CuO in the synthesized CPA/N-SWCNTs-GO-CE/CuO nanocomposites. The Raman spectra of CuO show three peaks at 571 cm^{-1}, 615 cm^{-1} and 895 cm^{-1}.

Mechanism of polymerization. According to the investigated results, a suggested mechanismto construct such modern hybrid nanocomposite is proposed to illustrate the fabrication method of CPA/N-SWCNTs-GO-CE/CuO nanocomposite (Fig. 8). The CPA/N-SWCNTs-GO-CE/CuO nanocomposite was synthesized by the softcopolymerization procedures using the chemical oxidative technique. The polymerization occurs in the presence of ANI with TPA and PPDA as cross-linkers with N-SWCNTs-GO-CE in an acidic medium. In the acidic environment, the -COOH groups on the surface of N-SWCNTs-GO-CE becomebe protonated, i.e., they gain H^+ from the medium[65]. Therefore, the adsorption of $SO_4^=$ anions may compensate for the positive charges on the N-SWCNTs-GO-CE surfaces and CuO NPs. Moreover, in the charge compensation method, additional adsorption of $SO_4^=$ on the N-SWCNTs-GO-CE and CuO NPs surface can work as the charge compensator for positively charged CPA chains in the formation of CPA/N-SWCNTs-GO-CE/CuO nanocomposite.ANI, PPDA and TPA are oxidized into cationic radicals under acidic environments using APS. Then, the polymerization of cationic radicals of ANI and PPDA creates poly(ANI-PPDA) as linear oligomers with two amino groupsis terminated.

The linear poly(ANI-PPDA) oligomer cationic radicals continue to react with TPA cationic radicals after oxidation tocompose a CPA network by polymerization at the three N para-positions due to similar reaction activities. Electrostatic interactions occur between cationic radicals withanions absorbed on both N-SWCNTs-GO-CE and CuO surface. Furthermore, it is conceivable that three types of hydrogen bonding occur: between chains of CPA and oxygen atoms on the N-SWCNTs-GO-CE surface,among the chains of CPA in the nanocomposite of CPA/N-SWCNTs-GO-CE/CuO, and between chains of CPA and oxygen atoms on the CuO surface. Finally, the π–π stacking between the π bonds of N-SWCNTs-GO-CE and the aromatic rings of CPA stabilizes the bound complex structure of the CPA/N-SWCNTs-GO-CE/CuO nanocomposite. The interactions can confirm that N-SWCNTs-GO-CE and CuO are inserted to produce core–shell structures and CPA chains[66–70]. Such above mentioned mechanism enhance the proposed charge transfer due to the use of such fabricated nanocomposites. The reported nanocomposited based on cross-linked PANI and coated with cellulose in the presence of mixed N-SWCNTs-GO nano-filler. In addition to the existence of CuO as well.

UV–Vis spectroscopic measurement for MO dye removal and photocatalytic degradation. MO has dual absorbance peaks at 277 and 466 nm. This dye shows high stability with distinguished absorption peaks in the absence of CPA/N-SWCNTs-GO-CE/CuO nanocatalyst. The rate of decolorization is approximately zero, and the photo-degradation doesnot entirely occur (see Fig. 9a). By using the CPA/N-SWCNTs-GO-CE/CuO nanocatalyst, we observe a substantial decrease in the main absorption peaks at 277 and 466. These changes are due tothe extensive mineralization of MO,which comprises the phenyl ring degradation. Furthermore, a considerable quenching at 466 nm occurs due to bleaching, which involves the azo bond cleavage (Fig. 9b). For additional investigation, the optical behaviour of the nanocatalyst-based CuO was examined using three conditions: under UV radiation, in the presence of (CPA/N-SWCNTs-GO-CE) and the combination of CPA/N-SWCNTs-GO-CE/CuO nanocatalyst under UV. The data analysis provides the photobleaching and degradation of the MO in the presence of the CPA/N-SWCNTs-GO-CE/CuO nanocatalyst under UV in the maximum time of 100 min. Moreover, the bleaching and photodegradation processes of MO completely disappear in the absence of the CPA/N-SWCNTs-GO-CE/CuO nanocatalyst. The results show that the adsorbability of MO on the nanocomposite surface does not change within 6 min after stirring the solution in the dark, and no further degradation occurs. Thus, with all conditions to investigate the adsorbability balance, the MO molecules and nanocomposite were stirred for approximately 10 min without light sources. Furthermore, Fig. 10 shows a smart summarized overview for the photocatalytic degradation process.

Effect of the solution pH on the catalytic process. The photocatalytic experimentation of the pH effect was investigated at a range of pH 4–10 using 50 mg of nanocomposite in 100 mL MO dye solution of 10 mg/L concentration at adjusted contact time. Moreover, different pH solutions were obtained using standard solutions of hydrochloric acid and sodium hydroxide. Figure 11 shows the pH effect on the proficiency of MO degradation and bleaching. The highest degradation and bleaching rates are detected at pH 6 (Fig. 11). These pH significances show that the degradation percentage increases with increasing pH up to 6; then, itbegins to quench. Generally, the pH effect on the degradation depending on the nanocomposite has been assorted with the establishment of acid–base equilibria to monitor the chemical behaviour of the nanocomposite surface[71,72]. Therefore, all following experiments were performed at pH 6. The pH effect on the adsorption and removal proficiency can be ascribed to the dissimilarity of Coulomb interactions between the CuO-based nanocomposite surfaces and MO.

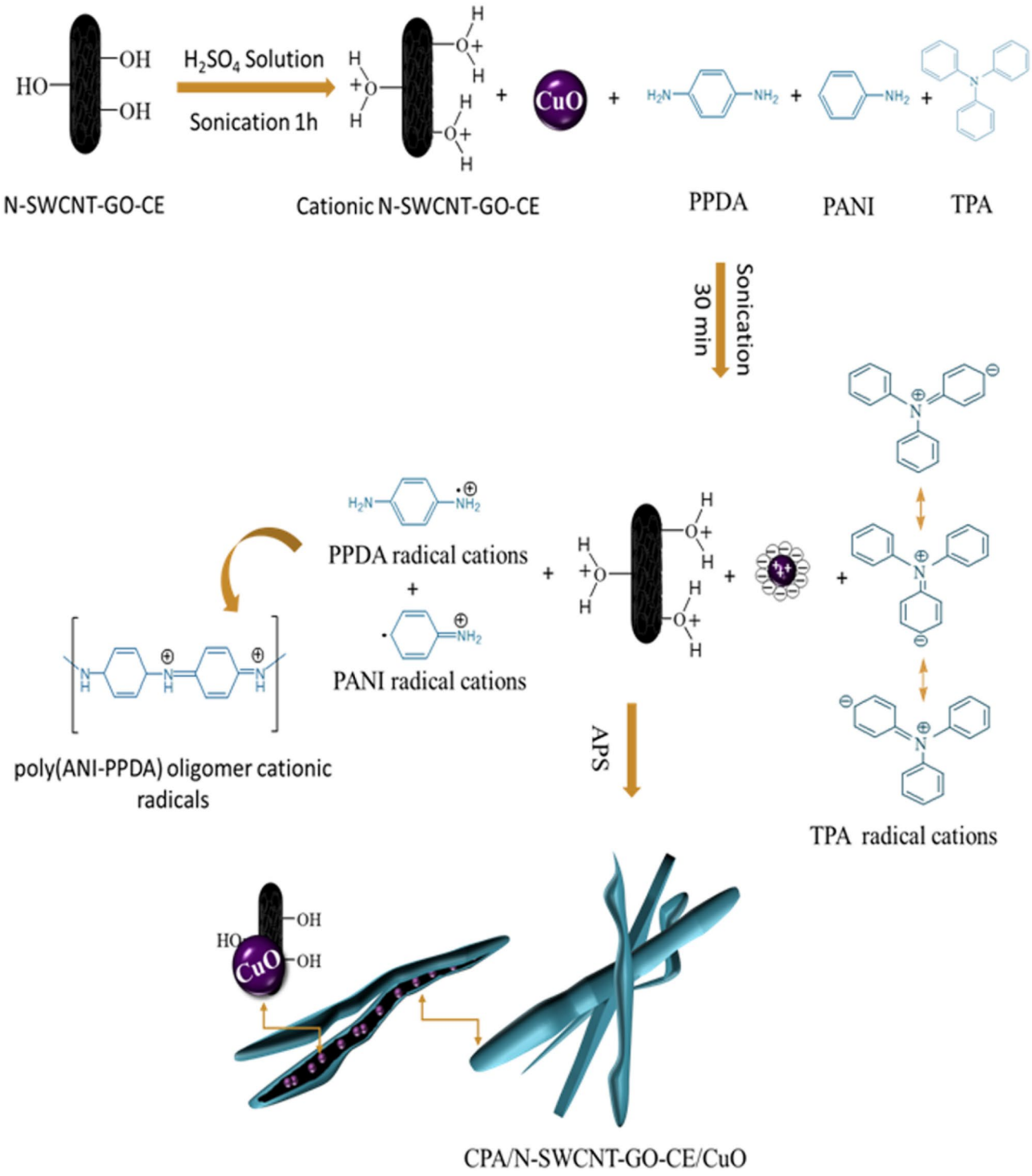

Figure 8. Illustration of the fabrication procedure of core–shell PAC/N-SWCNTs-GO-CE/CuO nanocomposites.

These interactions tend to enhance the adsorbability of MO molecules to the nanocomposite surfaces[73] and quench in the acidic medium due to the driving forces[74].

Additionally, MO has a pKa value of approximately 3.8[75]. In excess of this pKa and with increased pH, MO provides anions, which make it more easily bind to the surface of the CuO-nanocomposite. Thus, when the pH of the medium increases to 6, the adsorbability and removal efficiencies increase. At pH > 6, the bleaching and degradation were enhanced, which can be attributed to the quenching of the oxidation potential of hydroxyl radical due to increased pH[76]. However, the increase in hydroxyl ions at pH > 6 fights with MO anions at the nanocomposite surface[77].

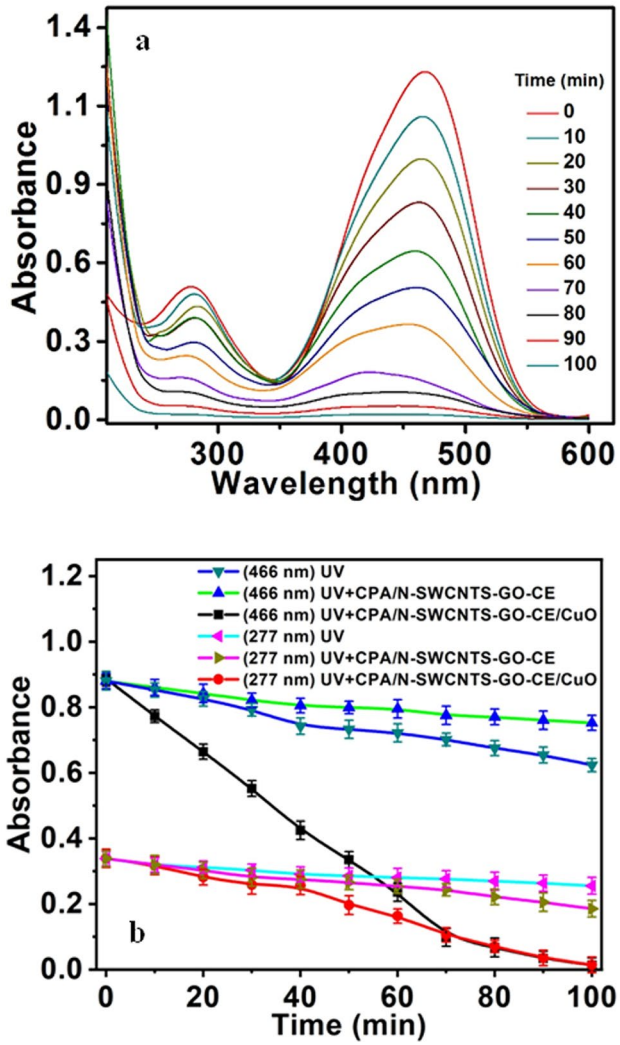

Figure 9. (**a**) photo-absorption spectral measurements of methyl orange in the presence of CPA/N-SWCNTs-GO-CE/CuO nano-catalysts using 50 mg/L nano-catalysts, MO 10 mg/L and at pH 6; (**b**) Alterations of the absorbance spectra versus time at wavelengths of 277 and 466 nm in three different cases UV radiation, in the presence of PCP-CNTs and nano-catalysts in presence of UV radiation.

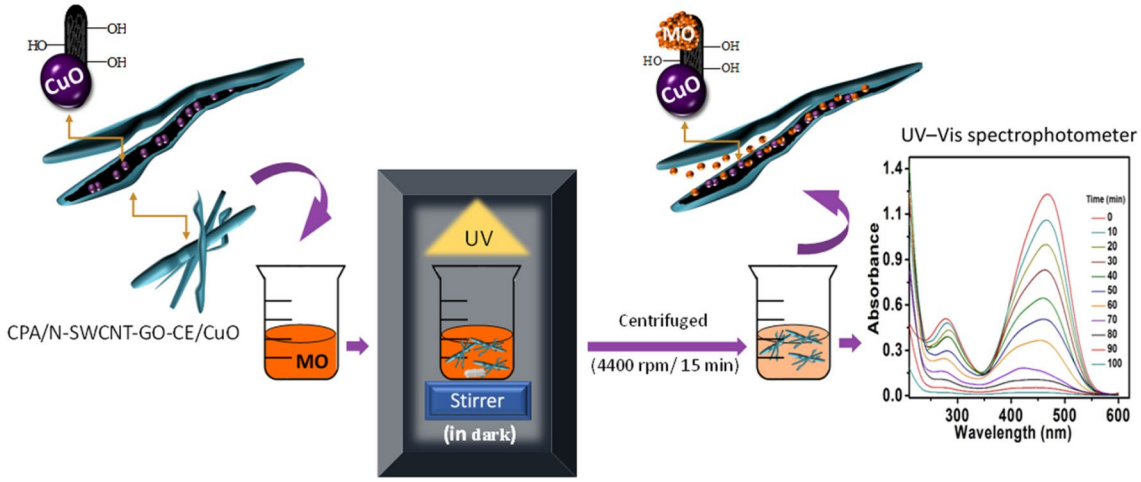

Figure 10. A smart overview for the photocatalytic degradation process og MO based on the CPA/N-SWCNTs-GO-CE/CuO nanocomposite.

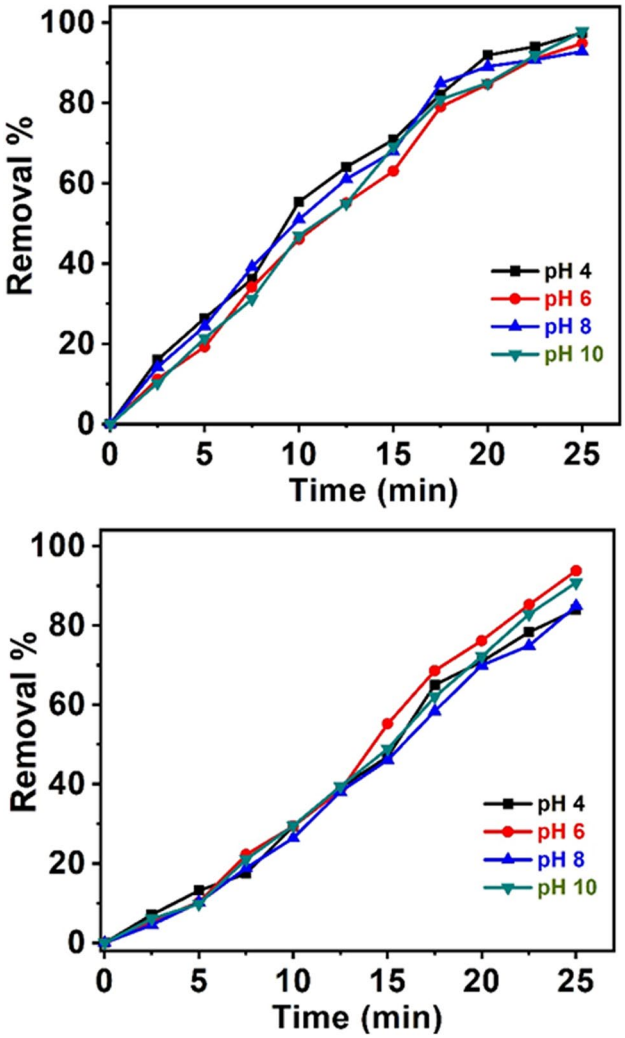

Figure 11. (**a**) pH effect on the bleaching process; (**b**) degradation efficiency of MO dye for 50 mg/L PCP-CNTs-Cu, MO 10 mg/L.

Effect of the CPA/N-SWCNTs-GO-CE/CuO nanocomposite dose. To investigate the effect of the nanocomposite dosage on the efficiency of bleaching and degradation of MO, different dosages of nanocomposite (25, 50,100 and 200 mg/L) were mixed with a solution containing 10 mg/L MO at pH 6 for 100 min. The obtained results are shown in Fig. 12. The data emphasize that the bleaching and degradation efficiencies increased with increasing nanocomposite content to 50 mg/L, exhibited no notable alteration when the nanocomposite weight increased to 100 mg/L, and extinguished when the nanocomposite quantity was 200 mg/L. This behaviour can be assigned to the presence of active sites, which increased with the increase in nanocomposite quantity. Consequently, the produced hydroxyl radicals enhanced the photocatalytic proficiency of the CuO-nanocomposite. With excess nanocomposite, the presence of a viscous colloid medium prevents UV light from penetrating the nanocomposite surface. Therefore, this effect inhibits the production of hydroxyl radicals and decreases the adeptness of MO deterioration and staining of the medium[78,79]. Thus, the nanocomposite quantity was adjusted to be 50 mg/L for further experimentation.

Effect of C_i of MO. To investigate the effect of MO dye on the degradation process, MO concentrations were utilized in the range of 5–20 mg/L throughout a reaction time of 100 min at pH of 6. In addition, the amount of nanocomposite is 50 mg/L. The results are shown in Fig. 13. The obtained data demonstrate that the bleaching and degradation decreased with increasing C_i of MO. This result can be related to the decrease in number of active sites of the CPA/N-SWCNTs-GO-CE/CuO nanocatalyst surface. Thus, the introduction of hydroxyl radicals quenches and reduces the competence of the photo-catalytic reaction. Meanwhile, the increase in C_i of MO reduces the photon path length that diffuses through the MO medium. With more MO molecules, the dye can absorb significantlymore light than the CPA/N-SWCNTs-GO-CE/CuO nanocomposite, which reduces the competence of the photo-catalytic degradation process[80,81]. Thus, the suitable C_i of MO is 10 mg/L.

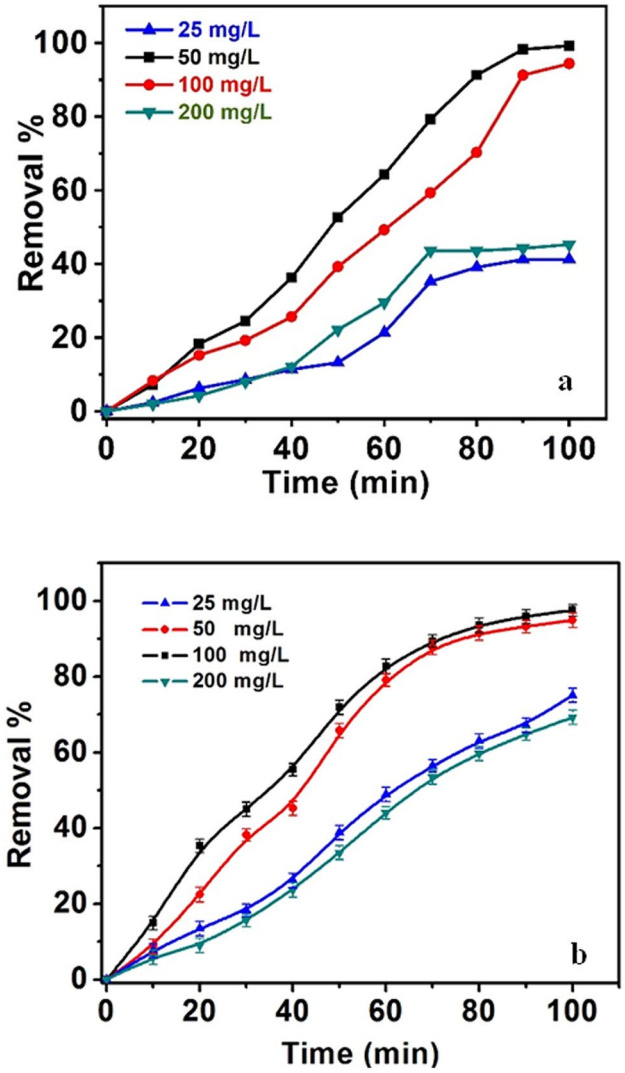

Figure 12. (**a**) Effect of CPA/N-SWCNTs-GO-CE/CuO nanospheres amount on the bleaching; (**b**) MO degradation, concentration of MO of 10 mg/L at pH 6.2 and time 100 min.

Oxygen content. The effect of oxygen was investigated on both bleaching and degradation of MO based on the CPA/N-SWCNTs-GO-CE/CuO nanocomposite surface. The studied solution was conducted to air and nitrogen atmosphere to study the oxygen effect on the degradation process. The experimentations were accomplished by monitoring several parameters: time of 100 min, pH 6, C_i of MO 10 mg/mL, CPA/N-SWCNTs-GO-CE/CuO nanocomposite concentration of 50 mg/mL, and the solution was exposed to nitrogen gas for 2.5 min. Figure 14 shows the oxygen gas effect on the rates of bleaching and degradation. Furthermore, the analysis of the obtained results indicates that the adequacy of bleaching and degradation enhances with oxygen. This resultcan be attributed to the introduction of reactive species including hydroxyl radicals, oxygen radical and hydrogen peroxide[82]. Thus, the resulting radicals increase the efficiency of bleaching and degradation of MO.

The proposed photocatalytic degradation mechanism. Schematic illustration explains the expected photocatalytic degradation mechanism for CPA/N-SWCNTs-GO-CE/CuO nanocomposite against MO dye has been given shortly in Fig. 15. Such photocatalytic decomposition of the azo dye on the CuO nanoparticles doped CPA/N-SWCNTS-GO-CE nanocatalysts under the UV radiation is presented in the following Fig. 15. Typically, the UV-radiation induces the valance band electrons of the CuO nanocatalysts convey to the conduction band. This equivalent energy is higher than the band gap of the doped CuO nanoparticles (2.43 eV)[83], thus disseminating the initiation electrons (e^-) of the conduction band and holes (h^+) of the valance band. The oxidation of the azo dyes could be presented straightforwardly by the generated holes or by the distinctive interaction of these holes with (OH^-) or H_2O to create hydroxyl radicals (OH·). Also, the induced electrons reduce oxygen molecules (O_2) adsorbed on the CPA/N-SWCNTS-GO-CE/CuO nanocomposite surface into superoxide (O_2^-) radicals. Finally, azo dyes were degraded by the induced OH· and $\cdot O_2^-$[84]. The significant interaction formulations are exhibited as follows:

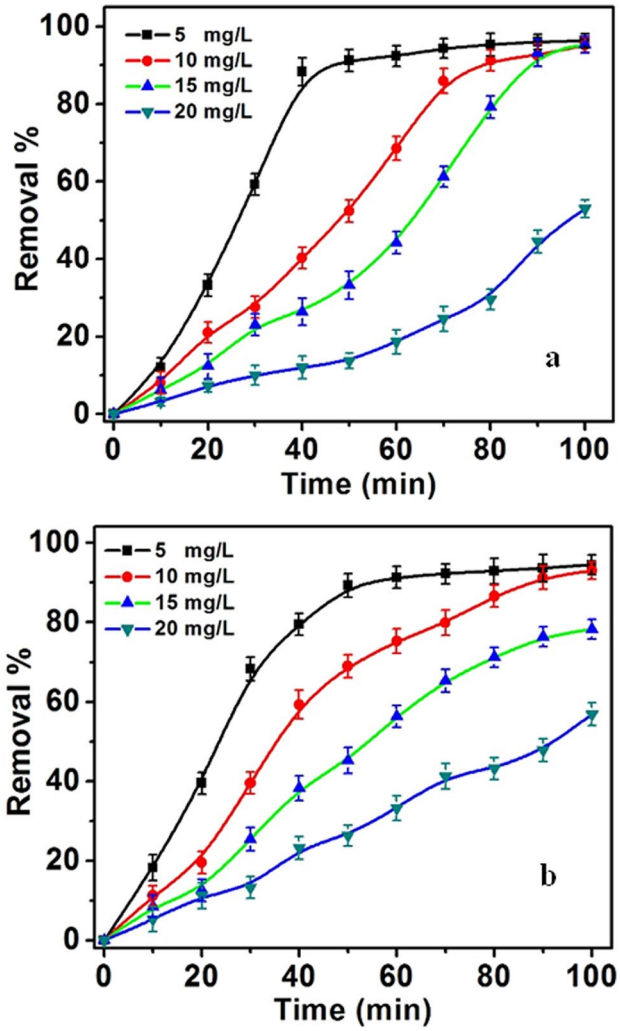

Figure 13. (**a**) Effect of initial concentration of MO on the bleaching; (**b**) degradation, the concentration of CPA/N-SWCNTs-GO-CE/CuO of 50 mg/L, pH 6.2 and time 100 min.

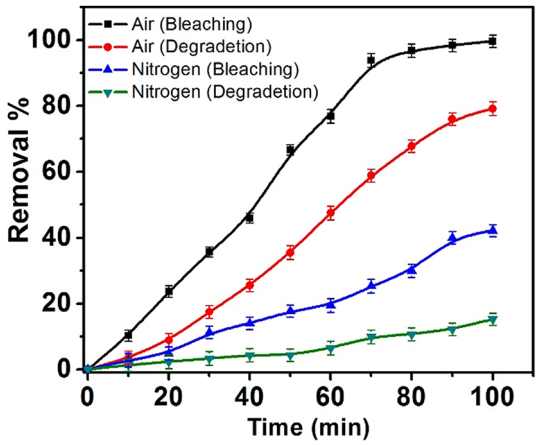

Figure 14. Oxygen effect on the rates of bleaching and degradation of MO at (time 100 min, pH = 6.2, the MO concentration of 10 mg/mL).

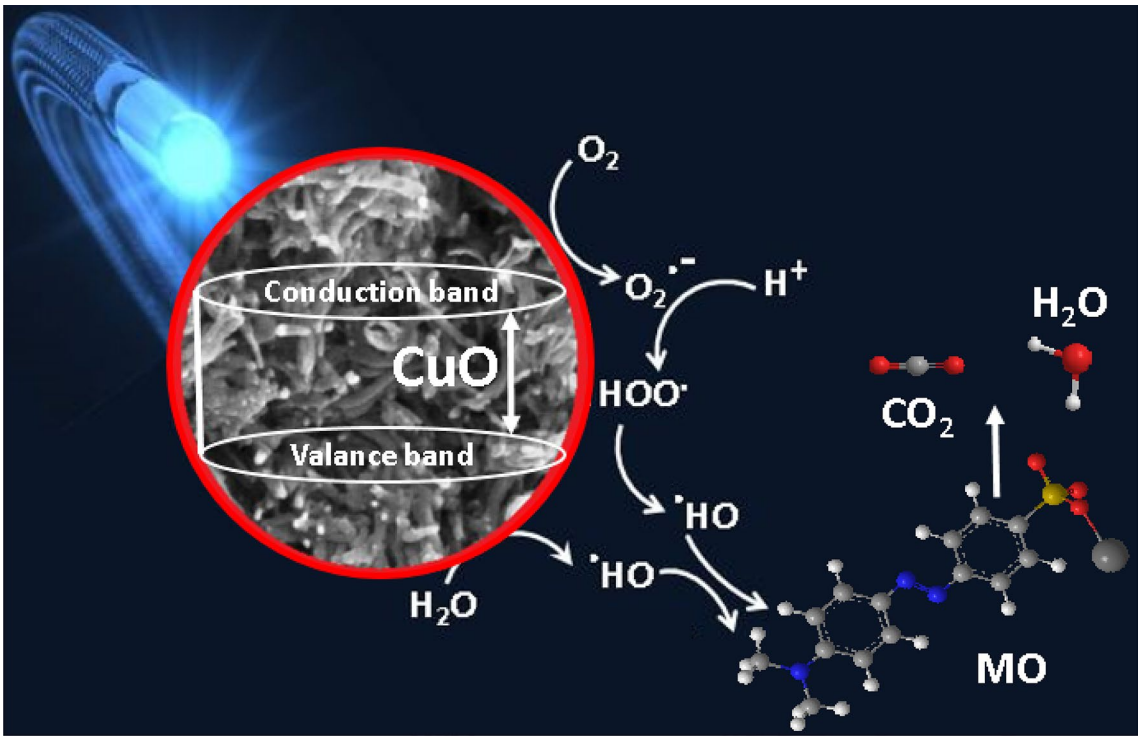

Figure 15. Reversibility of CPA/N-SWCNTs-GO-CE/CuO particles based on the bleaching and degradation rates of MO dye.

$$\text{nanocomposite doped CuO} + h\nu \rightarrow h^+ + e^-$$
$$\left(OH^-\right) \text{ or } H_2O + h^+ \rightarrow OH\cdot$$
$$(O_2) + e^- \rightarrow \cdot O_2^-$$
$$OH\cdot \text{ and } \cdot O_2^- + \text{Azo dyes} \rightarrow CO_2 + H_2O$$

In fact, the photo degradation process of the azo dye is mainly based on the chemical decomposition of MO molecules in the presence of $\cdot O_2^-$[83,84].

Reversibility of the CPA/N-SWCNTs-GO-CE/CuO nanocatalyst. The reversibility of the CPA/N-SWCNTs-GO-CE/CuO nanocatalyst has a noteworthy effect from the economic viewpoint. Therefore, it is essential to study the competence of the nanocatalyst throughout the recovery process. Thus, the used CPA/N-SWCNTs-GO-CE/CuO nanocomposite was collected after the bleaching and degradation processes using a centrifuge with an adapted rate of 4400 rpm. Then, the centrifuged nanocatalyst yield was washed three times with ethanol and bi-distilled water. The separated nanocatalyst was dried and reused in more processes as shown in Fig. 16. The effectiveness of the MO bleaching and degradation reduce with the amount of recovered CPA/N-SWCNTs-GO-CE/CuO catalysts. In addition, the quenching of the degradation rate is elevated than the bleaching process.

Furthermore, comparable studies of using different adsorbent against methyl orange removal at the optimum conditions have been given in Table 2. The results confirm the extreme higher efficiency of CPA/N-SWCNTs-GO-CE/CuO nanocomposite compared to the other reported materials.

Conclusion

In this work, a novel CPA/N-SWCNTS-GO-CE/CuO nanocomposite was successfully prepared via an oxidative chemical polymerization method. The core–shell structure was clearly visualized through TEM, SEM, XRD, FT-IR and RAMAN studies. These synthesized nanocomposites were utilized to remove a hazardous dye (MO) and found to be highly efficient in its removal. Various parameters that affect the adsorption process, including C_i of MO, pH and dosage of CuO-based nanocomposite, were optimized. In addition, the oxygen content has a significant effect on the degradation process. The obtained data clarified that the dye was successfully degraded in the presence of CPA/N-SWCNTS-GO-CE/CuO compared to CPA/N-SWCNTs-GO-CE under UV radiation, which indicates the enhanced effect of CuO as a reinforced agent. The degradation process was investigated under the optimal conditions of pH of 6, 50 mg/L of CPA/N-SWCNTS-GO-CE/CuO photocatalyst, C_i of MO of 10 mg/L and under stirring at room temperature in atmosphere. This high efficiency of the CuO NP-based nanocomposite as a photocatalyst may provide a promising application for the degradation of dyes from aqueous solutions. In addition, the CPA/N-SWCNTS-GO-CE/CuO catalyst exhibits significant reversibility and highly

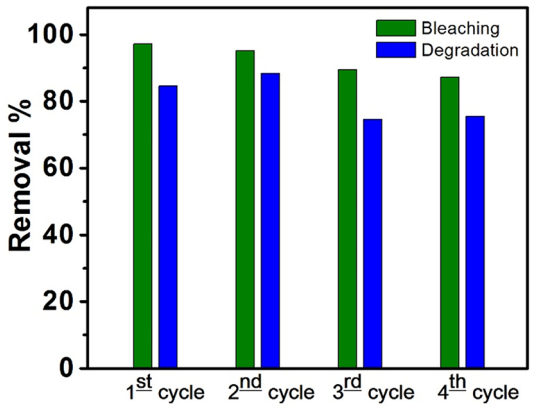

Figure 16. The proposed photodegradation mechanism of MO based CPA/N-SWCNTS-GO-CE/CuO under UV-light irradiation.

Adsorbent	Temperature	Time	pH	Efficiency	Ref
Biochar from pomelo peels	25 °C	70 min	3	–	[85]
Activated carbon from shaddock peels	25 °C	150 min	3	54.25%	[86]
poly(3,4-ethylene dioxythiophene) (PEDOT)-modified polyvinylidene fluoride electrospun fibers	50 °C	360 min	3	75%	[87]
ZIF-67@CoAl-LDH	25 °C	90 min	3	72.3%	[88]
$MnFe_2O_4$@CPB/H_2O_2/visible LED light	25 °C	150 min	3	99.5%	[89]
Gd_2O_3/Bi_2O_3@GO	35 °C	45 min	6	95%	[90]
CPA/N-SWCNTS-GO-CE/CuO + UV light	25 °C	100 min	6	100%	Current study

Table 2. Comparable studies of using different adsorbent in methyl orange removal at the optimum conditions.

recovered by effortless methods. This CuO-based photocatalyst provide an effective procedure with considerable effect in the wastewater treatment from dye pollution. Therefore, the present study has shown a simple and facile way for the synthesis of Cu NPs for the treatment of wastewater problems.

Novelty of the work

The authors confirm this research work is novel and has not been published or sent for publication in another journal.

Received: 1 December 2020; Accepted: 8 February 2021
Published online: 03 March 2021

References

1. Murray, K. E., Thomas, S. M. & Bodour, A. A. Prioritizing research for trace pollutants and emerging contaminants in the freshwater environment. *Environ. Pollut.* **158**, 3462–3471 (2010).
2. Hussein, M. A., Albeladi, H. K., Elsherbiny, A. S., El-Shishtawy, R. M. & Al-romaizan, A. N. Cross-linked poly(methyl methacrylate)/multiwall carbon nanotube nanocomposites for environmental treatment. *Adv. Polym. Technol.* **37**, 3240–3251 (2018).
3. Radoor, S., Karayil, J., Jayakumar, A., Parameswaranpillai, J. & Siengchin, S. Efficient removal of methyl orange from aqueous solution using mesoporous ZSM-5 zeolite: Synthesis, kinetics and isotherm studies. *Colloids Surf. A* **611**, 125852 (2021).
4. Tella, A. C. *et al.* Synthesis and crystal structures of zinc(II) coordination polymers of trimethylenedipyridine (tmdp), 4-nitrobenzoic (Hnba) and 4-biphenylcarboxylic acid (Hbiphen) for adsorptive removal of methyl orange from aqueous solution. *Polyhedron* **192**, 114819 (2020).
5. Nazri, M. K. H. M., Sapawe, N. Removal of methyl orange over low-cost silica nanoparticles extrated from bamboo leaves ash. *Mater. Today: Proc.* **2020** (Article in press). https://doi.org/10.1016/j.matpr.2020.10.969
6. Forgacs, E., Cserháti, T. & Oros, G. Removal of synthetic dyes from wastewaters: a review. *Environ. Int.* **30**, 953–971 (2004).
7. Alsbaiee, A. *et al.* Rapid removal of organic micropollutants from water by a porous β-cyclodextrin polymer. *Nature* **529**, 190–194 (2016).
8. Alqarni, S. A., Hussein, M. A., Ganash, A. A. & Khan, A. Composite material-based conducting polymers for electrochemical sensor applications: a mini review . *BioNanoScience.* **2020**, 1–14 (2020).
9. Ma, J. *et al.* Fabrication of PANI-TiO_2/rGO hybrid composites for enhanced photocatalysis of pollutant removal and hydrogen production. *Renewable Energy* **156**, 1008–1018 (2020).
10. JianYu, Z. *et al.* Wei, Cotton fabric finished by PANI/TiO_2 with multifunctions of conductivity, anti-ultraviolet and photocatalysis activity. *Appl. Surf. Sci.* **470**, 84–90 (2019).
11. Liao, G., Chen, S., Quan, X., Zhang, Y. & Zhao, H. Remarkable improvement of visible light photocatalysis with PANI modified core–shell mesoporous TiO2 microspheres. *Appl. Catal. B* **102**, 126–131 (2011).

12. Rahman, K. H. & Kar, A. K. Effect of band gap variation and sensitization process of polyaniline (PANI)-TiO2 p-n heterojunction photocatalysts on the enhancement of photocatalytic degradation of toxic methylene blue with UV irradiation. *J. Environ. Chem. Eng.* **8**, 104181 (2020).
13. Nekooie, R., Shamspur, T. & Mostafavi, A. Novel CuO/TiO2/PANI nanocomposite: Preparation and photocatalytic investigation for chlorpyrifos degradation in water under visible light irradiation. *J. Photochem. Photobiol. A: Chem.* **407**, 113038 (2021).
14. Yang, Y., Chen, S. & Xu, L. Enhanced conductivity of polyaniline by conjugated crosslinking. *Macromol. Rapid Commun.* **32**, 593–597 (2011).
15. Ganash, A. A., Alqarni, S. A. & Hussein, M. A. Poly(aniline-co-o-anisidine)/graphene oxide Au nanocomposites for dopamine electrochemical sensing application . *J. Appl. Electrochem.* **49**, 179–194 (2019).
16. Heng, B. *et al.* Rapid synthesis of CuO nanoribbons and nanoflowers from the same reaction system, and a comparison of their supercapacitor performance. *RSC Adv.* **3**, 15719–15726 (2013).
17. Chang, S. P. & Yang, T. H. Sensing Performance of EGFET pH Sensors with CuO Nanowires Fabricated on Glass Substrate. *Int. J. Electrochem. Sci.* **7**, 5020–5027 (2012).
18. Zhang, Q. *et al.* CuO nanostructures: Synthesis, characterization, growth mechanisms, fundamental properties, and applications. *Prog. Mater. Sci.* **60**, 208–337 (2014).
19. Zhong, M. L. *et al.* Synthesis, growth mechanism and gas-sensing properties of large-scale CuO nanowires. *Acta Mater.* **58**, 5926–5932 (2010).
20. Salavagione, H. J., Díez-Pascual, A. M., Lázaro, E., Vera, S. & Gómez-Fatou, M. A. Chemical sensors based on polymer composites with carbon nanotubes and graphene: the role of the polymer. *J. Mater. Chem. A* **2**, 14289–14328 (2014).
21. Wang, C. *et al.* Controlled synthesis of micro/nanostructured CuO anodes for lithium-ion batteries. *Nano Energy* **9**, 334–344 (2014).
22. Bennici, S. & Gervasini, A. Catalytic activity of dispersed CuO phases towards nitrogen oxides (N2O, NO, and NO2). *Appl. Catal. B Environ.* **62**, 336–344 (2006).
23. Umadevi, M. & Jegatha Christy, A. Synthesis, characterization and photocatalytic activity of CuO nanoflowers. Spectrochim. Acta - Part A Mol. *Biomol. Spectrosc.* **109**, 133–137 (2013).
24. Singh, J., Manna, A. K. & Soni, R. K. Sunlight driven photocatalysis and non-enzymatic glucose sensing performance of cubic structured CuO thin films. *Appl. Surf. Sci.* **530**, 147258 (2020).
25. Singh, J. & Soni, R. K. Controlled synthesis of CuO decorated defect enriched ZnO nanoflakes for improved sunlight-induced photocatalytic degradation of organic pollutants. *Appl. Surf. Sci.* **521**, 146420 (2020).
26. Anandan, S., Wen, X. & Yang, S. Room temperature growth of CuO nanorod arrays on copper and their application as a cathode in dye-sensitized solar cells. *Mater. Chem. Phys.* **93**, 35–40 (2005).
27. Mageshwari, K. & Sathyamoorthy, R. Flower-shaped CuO nanostructures: synthesis, characterization and antimicrobial activity. *J. Mater. Sci. Technol.* **29**, 909–914 (2013).
28. Kochmann, S., Hirsch, T. & Wolfbeis, O. S. Graphenes in chemical sensors and biosensors. *TrAC - Trends Anal. Chem.* **39**, 87–113 (2012).
29. Pérez-López, B. & Merkoçi, A. Carbon nanotubes and graphene in analytical sciences. *Microchim. Acta* **179**, 1–16 (2012).
30. Kargarzadeh, H. *et al.* Recent developments on nanocellulose reinforced polymer nanocomposites: A review. *Polym. (Guildf)* **132**, 368–393 (2017).
31. Hegde, M. S., Nagaveni, K. & Roy, S. Synthesis, structure and photocatalytic activity of nano TiO_2 and nano $Ti_{1-x}M_xO_{2-\delta}$ (M = Cu, Fe, Pt, Pd, V, W, Ce, Zr). *Pramana J. Phys.* **65**, 641–645 (2005).
32. Khedr, M. H., Abdel Halim, K. S. & Soliman, N. K. Synthesis and photocatalytic activity of nano-sized iron oxides. *Mater. Lett.* **63**, 598–601 (2009).
33. Anbuvannan, M., Ramesh, M., Viruthagiri, G., Shanmugam, N. & Kannadasan, N. Synthesis, characterization and photocatalytic activity of ZnO nanoparticles prepared by biological method. . *Spectrochim. Acta - Part A Mol Biomol. Spectrosc.* **143**, 304–308 (2015).
34. Mohan, D., Singh, K. P., Singh, G. & Kumar, K. Removal of dyes from wastewater using flyash, a low-cost adsorbent. *Ind. Eng. Chem. Res.* **41**, 3688–3695 (2002).
35. Jiangning, W., Mark, A. E. & Edward, S. L. Evaluation of membrane filtration and ozonation processes for treatment of reactive-dye wastewater. *J. Environ. Eng. ASCE* **1**, 272–277 (1998).
36. Saleh, S. M. ZnO nanospheres based simple hydrothermal route for photocatalytic degradation of azo dye. . *Spectrochim. Acta - Part A Mol Biomol. Spectrosc.* **211**, 141–147 (2019).
37. Nezamzadeh-Ejhieh, A. & Karimi-Shamsabadi, M. Comparison of photocatalytic efficiency of supported CuO onto micro and nano particles of zeolite X in photodecolorization of Methylene blue and Methyl orange aqueous mixture. *Appl. Catal. A Gen.* **477**, 83–92 (2014).
38. Horikoshi, S., Watanabe, N., Onishi, H., Hidaka, H. & Serpone, N. Photodecomposition of a nonylphenol polyethoxylate surfactant in a cylindrical photoreactor with TiO2 immobilized fiberglass cloth. *Appl. Catal. B Environ.* **37**, 117–129 (2002).
39. Wang, S. *et al.* CTAB-assisted synthesis and photocatalytic property of CuO hollow microspheres. *J. Solid State Chem.* **182**, 1088–1093 (2009).
40. Zhao, W. *et al.* Photodegradation of Sulforhodamine-B Dye in Platinized Titania Dispersions under Visible Light Irradiation: Influence of Platinum as a Functional Co-catalyst. *J. Phys. Chem. B.* **106**, 5022–5028 (2002).
41. Abu-Zied, B. M., Hussein, M. A., Khan, A. & Asiri, A. M. Cu-Cu2O@graphene nanoplatelets nanocomposites: facile synthesis, characterization, and electrical conductivity properties. *Mater. Chem. Phys.* **2018**(213), 168–176 (2018).
42. Alizadeh-Gheshlaghi, E., Shaabani, B., Khodayari, A., Azizian-Kalandaragh, Y. & Rahimi, R. Investigation of the catalytic activity of nano-sized CuO, Co_3O_4 and $CuCo_2O_4$ powders on thermal decomposition of ammonium perchlorate. *Powder Technol.* **217**, 330–339 (2012).
43. Alqarni, S. A., Hussein, M. A. & Ganash, A. A. Highly sensitive and selective electrochemical determination of sunset yellow in food products based on AuNPs/PANI-co-PoAN-co-PoT/GO/Au electrode. *ChemistrySelect.* **3**, 13167–13177 (2018).
44. Hussein, M. A., Ganash, A. A. & Alqarni, S. A. Electrochemical sensor-based gold nanoparticle/poly (aniline-co-o-toluidine)/graphene oxide nanocomposite modified electrode for hexavalent chromium detection: a real test sample. *Polym.-Plast. Technol. Mater.* **58**, 1423–1436 (2019).
45. Hussein, M. A., El-Shishtawy, R. M. & Obaid, A. Y. The impact of graphene nano-plates on the behavior of novel conducting polyazomethine nanocomposites. *RSC Adv.* **7**, 9998–10008 (2017).
46. Hussein, M. A., Abu-Zied, B. M. & Asiri, A. M. Fabrication of EPYR/GNP/MWCNT carbon-based composite materials for promoted epoxy coating performance. *RSC Adv.* **8**, 23555–23566 (2018).
47. Shahriary, L. & Athawale, A. A. Graphene oxide synthesized by using modified Hummers approach. *Int. J. Renew. Energy Environ. Eng.* **2**, 58–63 (2014).
48. Katowah, D. F., Mohammed, G. I., Al-Eryani, D. A., Sobahi, T. R. & Hussein, M. A. Rapid and sensitive electrochemical sensor of cross-linked polyaniline/oxidized carbon nanomaterials core-shell nanocomposites for determination of 2,4-dichlorophenol. *PLoS ONE* **15**(6), e0234815 (2020).
49. Katowah, D. F. *et al.* Fabrication of conductive cross-linked polyaniline/G-MWCNTS core-shell nanocomposite: A selective sensor for trace determination of chlorophenol in water samples. *Polym. Adv. Technol.* **31**(11), 2615–2631 (2020).

50. Nekouei, S. & Nekouei, F. Comparative procedure of photodegradation of methylene blue using N doped activated carbon loaded with hollow 3D flower like ZnS in two synergic phases of adsorption and catalytic. *J. Photochem. Photobiol. A Chem.* **364**, 262–273 (2018).
51. Hou, P.-X. *et al.* Synthesis of high quality nitrogen-doped single-wall carbon nanotubes. *Sci. China Mater.* **58**, 603–610 (2015).
52. Wang, X. *et al.* Crosslinked polyaniline nanorods with improved electrochemical performance as electrode material for supercapacitors. *J. Mater. Chem. A* **2**, 12323–12329 (2014).
53. Badawi, H. M., Förner, W. & Ali, S. A. A comparative study of the infrared and Raman spectra of aniline and o-, m-, p-phenylenediamine isomers. *Spectrochim. Acta - Part A Mol Biomol. Spectrosc.* **112**, 388–396 (2013).
54. Wang, J. J., Jiang, J., Hu, B. & Yu, S. H. Uniformly shaped poly(p-phenylenediamine) microparticles: shape-controlled synthesis and their potential application for the removal of lead ions from water. *Adv. Funct. Mater.* **18**, 1105–1111 (2008).
55. Lakouraj, M. M., Zare, E. N. & Moghadam, P. N. Synthesis of novel conductive poly(p-phenylenediamine)/ Fe3O4 nanocomposite via emulsion polymerization and investigation of antioxidant activity. *Adv. Polym. Technol.* **33**, 1–7 (2014).
56. Archana, S. & Jaya, S. R. Synthesis and characterization of poly (p-phenylenediamine) in the presence of sodium dodecyl sulfate. *Res. J. Chem. Sci.* **4**, 60–67 (2014).
57. Lu, X. *et al.* Mechanistic investigation of the graphene functionalization using p-phenylenediamine and its application for supercapacitors. *Nano Energy* **17**, 160–170 (2015).
58. Li, T. *et al.* Synthesis, characterization, and properties of aniline-p-phenylenediamine copolymers. *High Perform. Polym.* **25**, 348–353 (2013).
59. Ju, X., Bowden, M., Brown, E. E. & Zhang, X. An improved X-ray diffraction method for cellulose crystallinity measurement. *Carbohydr. Polym.* **123**, 476–481 (2015).
60. Kumar, T. H. V. & Sundramoorthy, A. K. Non-enzymatic electrochemical detection of urea on silver nanoparticles anchored nitrogen-doped single-walled carbon nanotube modified electrode. *J. Electrochem. Soc.* **165**, B3006–B3016 (2018).
61. Dresselhaus, M. S., Dresselhaus, G., Saito, R. & Jorio, A. Raman spectroscopy of carbon nanotubes. *Phys. Rep.* **409**, 47–99 (2005).
62. Bhattacharya, P. *et al.* Graphene decorated with hexagonal shaped M-type ferrite and polyaniline wrapper: a potential candidate for electromagnetic wave absorbing and energy storage device applications. *Rsc Adv.* **4**, 17039–17053 (2014).
63. Luo, J., Zuo, Y., Shen, P., Yan, Z. & Zhang, K. Excellent microwave absorption properties by tuned electromagnetic parameters in polyaniline-coated $Ba_{0.9}La0.1Fe_{11.9}Ni_{0.1}O_{19}$/ reduced graphene oxide nanocomposites. *RSC Adv.* **7**, 36433–36443 (2017).
64. Holzinger, M. *et al.* Functionalization of single-walled carbon nanotubes with (R-)oxycarbonyl nitrenes. *J. Am. Chem. Soc.* **125**, 8566–8580 (2003).
65. Shih, C.-J., Lin, S., Sharma, R., Strano, M. S. & Blankschtein, D. Understanding the pH-dependent behavior of graphene oxide aqueous solutions: a comparative experimental and molecular dynamics simulation study. *Langmuir* **28**, 235–241 (2012).
66. Wang, X. *et al.* Crosslinked polyaniline nanorods with improved electrochemical performance as electrode material for supercapacitors. *J. Mater. Chem. A.* **2**, 12323–12329 (2014).
67. Katowah, D. F. *et al.* Ternary nanocomposite based poly (pyrrole-co-O-toluidine), cobalt ferrite and decorated chitosan as a selective Co^{2+} cationic sensor. *Compos. B Eng.* **175**, 107175 (2019).
68. Katowah, D. F. *et al.* Poly (pyrrole-co-o-toluidine) wrapped $CoFe_2O_4$/R (GO–OXSWCNTs) ternary composite material for Ga^{3+} sensing ability. *RSC Adv.* **9**, 33052–33070 (2019).
69. Katowah, D. F. *et al.* Fabrication of hybrid PVA-PVC/SnZnOx/SWCNTs nanocomposites as Sn^{2+} ionic probe for environmental safety. *Polym.-plast. Technol. Mater.* **00**, 1–16 (2019).
70. Meshram, S. P., Adhyapak, P. V., Mulik, U. P. & Amalnerkar, D. P. Facile synthesis of CuO nanomorphs and their morphology dependent sunlight driven photocatalytic properties. *Chem. Eng. J.* **204–205**, 158–168 (2012).
71. Yang, T.C.-K., Wang, S.-F., Tsai, S.H.-Y. & Lin, S.-Y. Intrinsic photocatalytic oxidation of the dye adsorbed on TiO_2 photocatalysts by diffuse reflectance infrared fourier transform spectroscopy. *Appl. Catal. B Environ.* **30**, 293–301 (2001).
72. Tanaka, K., Padermpole, K. & Hisanaga, T. Photocatalytic degradation of commercial azodyes. *Water Res.* **34**, 327–333 (2000).
73. Rathore, B. S., Chauhan, N. P. S., Rawal, M. K., Ameta, S. C. & Ameta, R. Chitosan–polyaniline–copper (II) oxide hybrid composite for the removal of methyl orange dye. *Poly Bull.* **1**, 1–18 (2019).
74. Lakkaboyana, S. K., Khantong, S., Asmel, N. K., Yuzir, A. & Yaacob, W. Z. W. Synthesis of copper oxide nanowires-activated carbon (AC@ CuO-NWs) and applied for removal methylene blue from aqueous solution: Kinetics, isotherms, and thermodynamics. *J Inorg Organomet. P.* **29**, 1658–1668 (2019).
75. Šťastná, M., Trávníček, M. & Šlais, K. New azo dyes as colored isoelectric point markers for isoelectric focusing in acidic pH region. *Electrophoresis* **26**, 53–59 (2005).
76. Lucas, M. S. & Peres, J. A. Decolorization of the azo dye reactive black 5 by fenton and photo-fenton oxidation. *Dyes Pigm.* **71**, 236–244 (2006).
77. Asl, M. N. *et al.* Adsorption of organic dyes using copper oxide nanoparticles: isotherm and kinetic studies. *Desalin Water Treat.* **57**, 25278–25287 (2016).
78. Dashamiri, S. *et al.* Ultrasonic enhancement of the simultaneous removal of quaternary toxic organic dyes by CuO nanoparticles loaded on activated carbon: central composite design, *kinetic and isotherm study*. *UltSonoch.* **31**, 546–557 (2016).
79. Hossaini, H., Moussavi, G. & Farrokhi, M. Oxidation of diazinon in cns-ZnO/LED photocatalytic process: catalyst preparation, photocatalytic examination, and toxicity bioassayof oxidation by-products. *Sep. Purif. Technol.* **174**, 320–330 (2017).
80. Zhang, L., Cheng, H., Zong, R. & Zhu, Y. Photocorrosion suppression of ZnO nanoparticles via hybridization with graphite-like carbon and enhanced photocatalytic activity. *J. Phys. Chem. C* **113**, 2368–2374 (2009).
81. Ahmad, M. *et al.* Photocatalytic, sonocatalytic and sonophotocatalytic degradation of Rhodamine B using ZnO/CNTs composites photocatalysts. *Ultrason. Sonochem.* **21**, 61–773 (2014).
82. Litter, M. I. Introduction to photochemical advanced oxidation processes for water treatment. In *Environmental photochemistry part II* 325–366 (Springer, Berlin, 2005).
83. Singh, J., Kumar, S. & Soni, R. K. Synthesis of 3D-MoS2 nanoflowers with tunable surface area for the application in photocatalysis and SERS based sensing. *J. Alloys Compounds* **849**, 156502 (2020).
84. Singh, J., Palsaniya, S. & Soni, R. K. Mesoporous dark brown TiO2 spheres for pollutant removal and energy storage applications. *Appl. Surf. Sci.* **527**, 146796 (2020).
85. Zhang, B., Wu, Y. & Cha, L. Removal of methyl orange dye using activated biochar derived from pomelo peel wastes: performance, isotherm, and kinetic studies. *J. Dispersion Sci. Technol.* **41**(1), 125–136 (2020).
86. Tao, X., Wu, Y. & Cha, L. Shaddock peels-based activated carbon as cost-saving adsorbents for efficient removal of Cr (VI) and methyl orange. *Environ. Sci. Pollut. Control Ser.* **26**(19), 19828–19842 (2019).
87. Da Silva, R. J. *et al.* Kinetics and thermodynamic studies of Methyl Orange removal by polyvinylidene fluoride-PEDOT mats. *J. Environ. Sci.* **100**, 62–73 (2021).
88. Nazir, M. A. *et al.* Surface induced growth of ZIF-67 at Co-layered double hydroxide: Removal of methylene blue and methyl orange from water. *Appl. Clay Sci.* **190**, 105564 (2020).
89. Wang, Z., Li, Y., Xie, X. & Wang, Z. Bifunctional $MnFe_2O_4$/chitosan modified biochar composite for enhanced methyl orange removal based on adsorption and photo-Fenton process. *Colloids Surfaces A: Physicochem. Eng. Aspects* **1**, 126104 (2020).
90. Das, T. R. & Sharma, P. K. Bimetal oxide decorated graphene oxide (Gd_2O_3/Bi_2O_3@GO) nanocomposite as an excellent adsorbent in the removal of methyl orange dye. *Mater. Sci. Semicond. Process.* **105**, 104721 (2020).

Author contributions

D.K. and M.H. suggested the design. D.K. prepared the materials. S.S., R.A. and G.M. displayed the photocatalytic activity. D.K. and M.H. collected the results. D.K., S.S., S.A., R.A. and G.M. prepare the figures. D.K. S.S. and S.A. wrote the main text. All authors reviewed the manuscript.

Competing interests

The authors declare no competing interests.

Additional information

Correspondence and requests for materials should be addressed to M.A.H.

Reprints and permissions information is available at www.nature.com/reprints.

Publisher's note Springer Nature remains neutral with regard to jurisdictional claims in published maps and institutional affiliations.